Characterizing reflector-feed interaction for parabolic reflector antennas

Mark A. Apeldoorn

January, 2011

TUDelft   **ASTRON**

Characterizing reflector-feed interaction for parabolic reflector antennas

Master Thesis

Author: Mark A. Apeldoorn
Student number: 1289586
Defence date: January 11, 2011

Committee members:

Prof. DSc. A.G. Yarovoy
Dr. M. Simeoni
Ir. W. A. van Cappellen (ASTRON)
Dr. D. Caratelli

International Research Centre for Telecommunications and Radar
Department of Telecommunications
Faculty of EEMCS
Delft University of Technology
P.O. Box 5031, 2600 GA Delft
The Netherlands

TUDelft   IRCTR   ASTRON

Abstract

The standing wave phenomenon is a plaguing phenomenon for spectroscopic observations in radio astronomy. The parabolic reflector antennas which are used for performing astronomical observations are wideband systems and therefore observers which have to deal with standing waves between the reflector and the feed. These standing waves complicate the calibration of radio telescopes and are a limiting factor of the dynamic range ('image quality') in wideband systems.

In this thesis we have investigated the reflector-feed interaction of a parabolic reflector antenna, by simulating and visualizing the standing waves between the reflector and the feed and the effect this phenomenon has on the antenna performance. We have studied different types of feeds (dipole-disk, horn and array feeds), each having different scattering properties. Hereby we have obtained a better understanding of the influence the feed scattering has on the antenna gain and the -3 dB beamwidth of the reflector antenna.

The radar cross section (RCS) of each feed has been analyzed and possibilities of reducing the RCS have been investigated. A lower feed RCS results in less feed scattering and therefore the multiple reflections between the reflector and the feed can be mitigated. Reflector-feed simulations have shown that the effect of the standing wave phenomenon, a fluctuating antenna gain and a varying -3 dB beamwidth of the reflector antenna, can be significantly reduced. By studying the RCS of different feeds and the effect the this has on the antenna performance a better understanding on the mitigation possibilities of the standing wave phenomenon has been obtained.

Acknowledgments

I am very glad to have had theo possibility to perform this research. It has given me the opportunity to combine my field of study with the field of astronomy, which I have found fascinating ever since I was little. I would therefore like to thank my supervisor, dr. Massimiliano Simeoni, for his assistance and daily support during the last year. His guidance has helped me to deliver this work.

I would like to pay my gratitude to ir. W. van Cappellen from ASTRON, from whom the idea of this research topic originated. The visits to ASTRON were a delight and it was nice to observe the Westerbork Synthesis Radio Telescope up-front.

The daily presence of my fellow students Hossein Azodi, Pablo Rodriquez and Wyger Brink was of great encouragement and created a nice working atmosphere. Thank you guys.

Last but not least, I would like to thank my parents for their support the last few years. And of course my girlfriend, who has alway been there to support me.

Mark Apeldoorn
Delft, December 22, 2010

"The history of astronomy is a history of receding horizons."
- Edwin P. Hubble, Realm of the Nebulae, 1936

Contents

Chapter 1

Introduction

1.1 General introduction

For more than 50 years radio astronomers have been using radio telescopes for observing and studying celestial objects. Before that time the only way observations were performed was by using optical telescopes. Optical telescopes collect (visible) light, which corresponds to the part of the electromagnetic spectrum that can be detected by the human eye. In the 1930s it was discovered that celestial objects could also be detected by performing observations in different parts of the electromagnetic spectrum [7] [8]. These objects are called radio sources and emit energy at frequencies which fall within the spectrum of radio waves. Radio waves have wavelengths from about one millimeter to hundreds of meters, corresponding to a frequency range of 3 MHz to 300 GHz. Electromagnetic waves produced by astronomical objects have wavelengths which lie within this range.
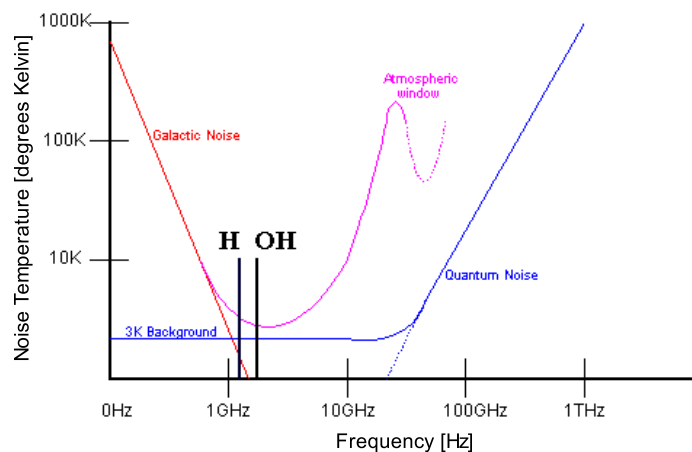

Figure 1.1: Frequencies at which radio astronomy suffers from sky noise, indicated by the amount of (additive) noise temperature (from http://www.setileague.org) [1].

Radio telescopes are designed to collect the energy emitted by these radio sources. One of the frequencies at which telescopes commonly observe is 1.42 GHz. At this frequency electromagnetic waves have a wavelength of about 21 cm. Hydrogen atoms are known to be radiating electromagnetic energy at a frequency of 1.42 GHz. In 1951, Ewen and Purcell [2] were the first to detect a spectral line at 1.42 GHz from measurement data obtained with a self constructed horn antenna at the Harvard University. Over a small range of the electromagnetic spectrum they were able to observe a (spectral) line, by measuring a power fluctuation, which indicated the presence of hydrogen. This spectral line is known as the hydrogen line. In 1945, astronomer H.C. van de Hulst [3] already suggested that hydrogen radiates electromagnetic energy at this frequency. By assuming that hydrogen atoms are uniformly distributed throughout a galaxy, one could for instance observe the presence of such a galaxy by detecting the hydrogen line. By taking multiple measurements, and thereby detecting multiple hydrogen lines, a slight change of frequency (or Doppler shift) could reveal the relative speed of a galaxy. Another advantage is that electromagnetic waves with a wavelength of 21 cm barely suffer noise contribution when for example they pass through the Earth's atmosphere. Figure 1.1 shows a frequency range at which electromagnetic waves suffer from interference from the Earth's atmosphere and from galactic and quantum noise. The interference is defined as the noise temperature $T = N/kB$ in Kelvin, where N is the noise power within bandwidth B, and $k = 1.38 \times 10^{-23} \mathrm{K}^{-1}$ is the Boltzmann's constant. Electromagnetic waves can pass through the Earth's atmosphere without suffering from too much interference within the 10 MHz to 10 GHz frequency range. Frequencies within this range are therefore favored in radio astronomy when observations are performed from the Earth's surface.

A few telescopes which are designed to operate at this preferred frequency range and that have been operational for more then 40 years are the Arecibo Radio Telescope in Puerto Rico (1963), the Nançay Decimetric Radio Telescope in France (1965) and the Westerbork Synthesis Radio Telescope in Dwingeloo, The Netherlands (1970) (all shown in Figure 1.2). Each of these telescopes is of a different design. Where the Arecibo telescopes is the largest (fixed) single-aperture off-axis aligned feed telescope with a reflector diameter of 305 meter, the Nançay telescope consists of a primary flat mirror positioned 460 meter away from the secondary fixed mirror. The Westerbork Synthesis Radio Telescope (WSRT) consists of an array of parabolic telescopes. To let the array operate as one big antenna, signals from all the telescopes are combined in a coherent way. This technique is commonly used in radio astronomy and is called interferometry. By combining the surfaces of all telescopes, an 'imaginary' huge single-dish telescope can be created through the aperture synthesis technique. The amount of collecting area would be smaller (and therefore less sensitive) than for instance the Arecibo telescope, but they are easier to construct. Although all three mentioned telescopes have a different configuration, they all focus the received energy to a focal point by using one of more large mirrors/reflectors.

Parabolic reflector antennas are the most commonly used for radio astronomy. Reflector dishes of radio telescopes are most of the time quite large. One reasons why large surface areas are preferred, is because of the large collecting area required to observe a radio source. By focusing more energy towards a focal point, where a receiving antenna is positioned, the gain of the telescope will increase. High antenna gains are required in order to observe the radio sources with a flux density smaller than 1 mJy. A source with a flux density of 10 Jy is considered a

(a) Arecibo Telescope

(b) Nançay Telescope

(c) Westerbork Synthesis Radio Telescope

Figure 1.2: Different types of telescopes used for radio astronomy.

sky source. This coincides with the fact that if a parabolic reflector antenna increases in size, the directivity of the antenna will also increase [4]. The beamwidth of the antenna will become narrower and the observed area in the sky can be observed at a higher resolution. Unfortunately, the large dimensions of radio telescopes and the weakness of the observed radio sources make them therefore very sensitive to noise and interferences.

1.2   Chromatism in radio telescopes

In 1977 Morris introduced the term of chromatism in radio telescopes [23]. Due to the incomplete absorption of the incident field by the receiver a *ripple* in the baseline of the observed spectrum was observed by Penzias and Scott [5] and Allen [6]. Allen [6] showed that the energy incident from a radio source could be reflected from a receiver input mismatch, re-radiated by the feed, and re-enter the receiver a second time after reflection at the apex of the telescope mirror.

The presence of chromatism in radio telescopes was first observed by van Woerden [7]. From 1956 to 1960 he performed hydrogen line observations with the Dwingeloo telescope (predecessor of the WSRT). Comparison of these measurement results acquired over the years showed systematic variations which he identified as stray radiation, radiation which entered the feed from a

different direction than the direction of observation. Several investigations have been performed on the Dwingeloo telescope by van Woerden et al. [8] and Raimond [9] in 1962 and 1966 respectively. They all concluded that the Dwingeloo telescope, and essentially all (parabolic) reflector antennas, experience chromatism.

Allen observed a fluctuation in the calibration data obtained with the Nançay telescope in 1969 [6]. He observed a varying gain and presumed this was caused by reflections on the primary mirror of the Nançay telescope. This *instrumental chromatism*, as he called it, was recognized as a gain variation over frequency. The measured period of this cyclic variation was 535 kHz. The focal length of the Nançay telescope is 280 meter. The period at which standing waves would be present can be calculated by $\Delta f = c/2F$, where c is the speed of light (in vacuum) and F the focal length of the main reflector. The expected standing wave period for the Nançay telescope would therefore be 535 kHz and this would seem to coincide with the gain variation. One important aspect mentioned by Allen is that the Nançay telescope would suffer less from the gain variation than smaller telescopes. Depending on the bandwidth measured, one would observe less cyclic variations over the same bandwidth when the focal length of a telescope is smaller. This makes it harder to detect them. As Allen mentioned, Penzias and Scott [5] were unsuccessful to eliminate the effect with the Green Bank telescope ($c/2F \cong 7.5$ MHz). The amplitude of these variations would, on the other hand, decrease since a smaller focal length would most of the time mean a smaller reflector and therefore a smaller antenna gain.

The cyclic variation in the measurement data was later identified as the standing wave phenomenon by Briggs et al. in [10] and is until today still a plaguing phenomenon for spectroscopic observations in radio astronomy. Briggs et al. analyzed survey data from the Arecibo and Nançay telescopes, which were for both acquired with a driftscan method. This is done by holding the telescope still while the Earth is rotating and the sky is observed. They were able to filter out the multiple reflections. This was done by identifying a reflected interfering signal as a signal which would enter the feed with a certain time delay after the original signal.

Popping and Braun performed their study on the WSRT telescopes [11]. By studying the WSRT they observed systematic oscillations in the beam properties as a function of frequency. This main beam fluctuation became known as *the heartbeat* of the WSRT [12]. The integrated beam area, the ratio of integrated side-lobe to main-lobe power and the effective aperture of the telescope system all seemed to be affected. The period of these oscillations is approximately 17 MHz. The focal length of a WSRT telescope is 8.75 m. With $\Delta f = c/2F$, they therefore assumed that the oscillations are closely tied to the presence of the standing waves between the reflector and the feed. Popping and Braun developed a frequency-resolved beam model which could be applied on the measurement data. With this model they have verified that they were able to deduce the oscillations in the beam properties. Unfortunately, this required a substantially increased complexity of data processing. Another disadvantage is that the total power measurements also suffer from the same effect and that there is no comparable correction procedure for this. They suggested that physically eliminating the reflections between the reflector and the feed is the only way to solve this. Suggestions they proposed are reported in Section 1.5.

1.3 Studies on feed scattering

Several analytical and numerical studies on the multiple reflections in radio telescopes, namely parabolic reflector antennas, have been performed. The approaches of these studied will be presented in Chapter 2. Where Morris [23] has taken a analytical approach, Kildal [13], Moldsvor and Kildal [14] [15] and Kildal, Skyttemyr and Kishk [16] have taken numerical approaches. The goals of the numerical approaches was to study the standing wave phenomenon, which they named *the resonance problem*, and change the physical parameters of the complete parabolic antenna to benefit from the effect. For their design a dipole-disk antenna feed with beamforming ring was used, shown in Figure 1.3 [17]. The dipole-disk is an antenna which consists of a dipole backed by a perfect electric conducting (PEC) disk and with a PEC ring placed in front of it. The purpose of the disk is to make it a directional antenna. The circular beamforming ring has the function of compressing the magnetic field pattern and is used to create a magnetic field pattern which is similar to the electric field pattern. In Section 3.1 this antenna will be described in more detail. Kildal presented a dipole-disk fed resonant reflector antenna of which the aperture efficiency is maximized by taking advantage of the multiple reflections between the feed and the reflector [13]. Besides changing the parameters of the dipole-disk (for example the size or placement of the disk), he also took the spacing between the feed and the reflector into consideration. With a center aligned feed, the position of the feed was changed towards or away from the apex of the reflector. The multiple reflections will then start to behave in a constructive manner if the right spacing is found and will result in a higher antenna gain for a narrow operating frequency. For different surrounding frequencies and with the same reflector-feed spacing, the antenna gain is not maximized. At some frequencies the multiple reflections will behave in a destructive manner and it is presumed that with the presence of standing waves the antenna gain drops to a local minimum.
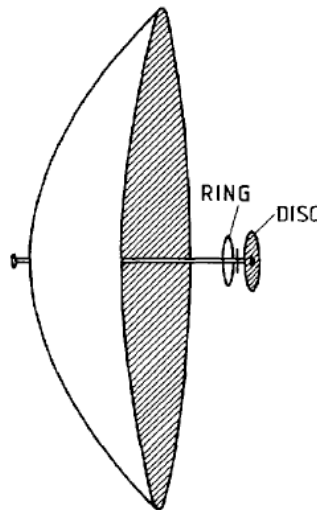

Figure 1.3: Dipole-disk fed resonant reflector antennas. [14]

1.4 Gain fluctuations in the WSRT

For a few years now The Netherlands Institute for Radio Astronomy (ASTRON) has been developing and testing a new type of feed for the WSRT, the Focal Plane Array (FPA) or Phased Array Feed (PAF) [19]. Figure 1.4 shows one of the FPA prototypes in place. The FPA consists of an array of Vivaldi radiating elements surrounded/backed by the same-sized feedbox as the one that is currently used for the traditional horn feeds. Currently the WSRT telescopes are equipped with Multiple Frequency Front Ends (MFFE). The MFFE consists of several corrugated horn which can be put into place by a rotation mechanism and are linear-, dual- and/or circular-polarized receivers. The feedbox blocks part of the aperture of the parabolic reflector. The fact that the feedbox is positioned in front of the parabolic reflector has to do with the fact that the received signals need to be amplified as close to the receiver as possible, since the measured signals are very sensitive to noise. The electronics needed for this are therefore placed at this point. More information about the WSRT receivers can be found in Appendix A.

With the use of the FPA feed the instantaneous field of view of the WSRT telescopes can be increase by a factor of 25 and will therefore significantly improve the survey speed [20] [21]. This is achieved by the fact that multiple beams can be formed instantaneously by a complex weighted sum of the FPA elements, where each element can be seen as an individual receiving antenna. Another benefit of the FPA feed is that measurements can now be performed with a higher antenna efficiency than previously possible.

Figure 1.4: One of the FPA prototypes positioned in the Westerbork Synthesis Radio Telescope.

Measurement results obtained with the FPA feed showed that the antenna gain fluctuation, which is assumed to be caused by the presence of the standing wave phenomenon, cannot be observed anymore. It was always thought that the effect of the standing wave phenomenon could not be (entirely) eliminated. In Figure 1.5 measurement results of the horn and FPA feed shown, where the gains are scaled to unity mean. From these results it can be observed that

the periodic variation over frequency in the antenna gain is present for the horn feed, but not for the FPA feed. The measurements were acquired by W. van Cappellen from ASTRON. The resonance frequency, which is about 17 MHz spacing between the local minima, again seems to be closely tied to the presence of standing waves. Since the focal length F of a WSRT telescope is 8.75 m, half a wavelength is present between the reflector and the feed at a frequency of 17 MHz ($c/2F$, where c is the speed of light). At every frequency which is a multiple of 17 MHz, an exact number of half-wavelengths will be present between reflector and feed.
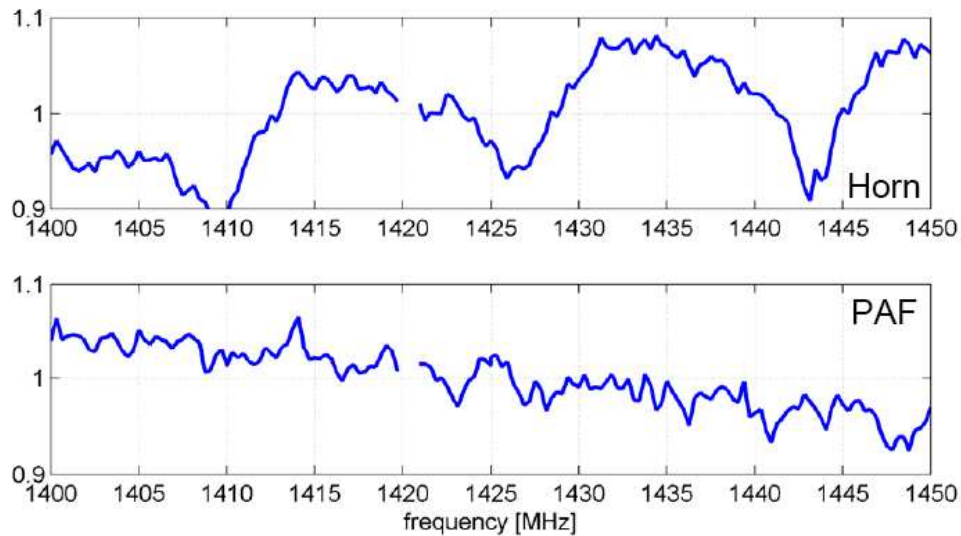

Figure 1.5: Fluctuation of the antenna gain over frequency measured with the WSRT [32].

Several practical solutions were tested on the WSRT with horn feeds to try to eliminate the standing wave phenomenon by suppressing the direct reflections between the feed and the apex of the reflector. One of the tests that have been performed was placing a tilted plate in the apex of the dish. This plate was placed under a slight off-axis angle, pointing with the flat side away from the feed. The intention was to remove the direct reflection between the feed and the apex of the dish. These tests were not successful and did not lead to the desired effect.

Another test performed was by placing electromagnetic absorber (cones) in the vertex of the dish to eliminate the reflections. This test led to the same results as for the plate. Another disadvantage of this solution was that the absorbers produced an increase in noise temperature. Since some of the receivers are cooled to operate at a fixed temperature, extra noise temperature could not be tolerated.

1.5 Objectives and outline of this thesis

As it was discussed above, the standing wave phenomenon seems to cause a significant and very complex frequency dependent variation of the antenna gain. This makes it very difficult to calibrate radio telescopes. Popping and Braun [11] suggested that prevention of the standing

waves in the WSRT telescopes could solve the problem of a variation in the total power measurements. This is the only effect that they could not account for through the post processing of the measurement data. By eliminating the presence of the standing waves, parabolic reflector antennas could be calibrated more accurately. Multiple reflections in primary feed telescopes are thought to be mainly caused by the surfaces of the feed and the support legs facing the reflector. If, to some extent, the scattering or reflections on these objects can be prevented, and the on-axis feed alignment can be kept, the calibration of parabolic reflector antenna will become much easier. Popping and Braun [11] suggested that one solution could be a surface treatment of the aforementioned surface areas to make them behave as broad-band isotropic scatterers. This would lead to a better result than to cover the surfaces of the feed and support legs with an absorbing material, since large absorbers will affect the system noise temperature.

That the effect of the standing wave phenomenon with the use of the FPA feed is not observable anymore, was not expected. It is presumed that the radar cross section (RCS) of the FPA feed is much lower than the RCS's of the currently used horn feeds and that therefore more energy is absorbed by the feed. In previous studies it was thought that the feed and the support legs both contributed to the phenomenon. A study of the relation between the effect of the standing wave phenomenon and the parameters of a feed, for instance the RCS, might shed some light on this matter. Therefore the reflector-feed interaction needs to be studies and characterized.

In the previously mentioned works the presence of the standing waves has been assumed. As far as we know, the interrelation between the standing waves between the reflector and the feed and the fluctuating gain has never been directly proven, through measurements or simulations. The first goals of this research would then be to confirm their their presence and effect on the antenna performance. One way to approach this goals is to analytically or numerically analyze a parabolic reflector antenna. Several methods and techniques have been researched and will be described in **Chapter 2**. Since radio telescopes are electrically large structures, it will be difficult to numerically simulate a full scale WSRT model. We will only focus our attention on studying an axial-feed parabolic reflector antenna. Cassegrain, Gregorian or off-axis fed reflector antennas are not taken into account, even though they might also be affected by the standing wave phenomenon. An axial-feed parabolic reflector antenna is a less complex structure to analyze (single reflector, primary fed reflector) and will have a symmetrical shape with the right feed. Even though the WSRT has dual-polarized receivers, we will consider only a single polarized feed.

Different possibilities of simulating the standing wave phenomenon will be discussed in **Chapter 3**. With the discussed approaches in **Chapter 2**, a model of a parabolic reflector antenna will be implemented and the simulation results will be presented.

To get a better understanding of the interaction between the reflector and the feed, it is important to study some feed characteristics. The feeds used for the WSRT telescopes, the corrugated horns (in the MFFE) and the FPA feed, are quite complex. In **Chapter 4** these feeds, together with a few simpler feeds, will be studied and simulated. From these results we will get a better understanding on their scattering behavior.

The simulations of real size telescopes acquires a lot of computational power. Radio tele-

scopes are most of the time quite large structures, compared to the wavelength of the signals they receive. In **Chapter 5** the possibilities of simulating parabolic reflector antennas are presented. Knowing that over the last few decades computers have become more and more powerful, a feasibility study will be performed to find out if nowadays large telescopes can be simulated.

Conclusions and recommendations of this thesis will be presented in **Chapter 6**. Is there a relation between the effect of the standing wave phenomenon and the parameters of the feed? If there is, can this be linked to the characteristics of the FPA feed used in the WSRT telescope?

The last chapter of this thesis will be the **Appendix**, where some complementary information will be presented.

Chapter 2

Study of the reflector-feed interaction

In the past the effect of the multiple reflections in radio telescopes has been studied extensively. To date, research on fully eliminating this effect has not been successful. This effect has been observed in the fluctuation of the antenna gain over frequency. A coherence between the fluctuating gain and the presence of standing waves between the reflector and the feed has been assumed in previous studies on radio telescopes, but has never actually been proven.

A lack of computational power and electromagnetic simulation tools has held back the research on this problem for a long time. In 1949, Silver already assumed the presence of multiple reflections which he presented in [22]. He concluded that this effect had a minimal influence on the antenna radiation pattern and could therefore be neglected. When it became clear that the multiple reflections did have an effect on the antenna performance, several analytical and numerical studies were performed. These will be presented in this chapter, followed by the approach followed for the reflector-feed interaction research that we have carried out.

2.1   Analytical approaches

In [23], Morris performed an analytical study on the chromatism in radio telescopes by introducing the feed scattering factor γ. He defines the scattering factor as follows. By considering a feed system illuminated by some incident field, part of the incident field will is absorbed by the feed and part will be reflected. The scattered field will be denoted by $\mathbf{E}_S$, which indicates the scattered field values at a distant observation point. By short-circuiting the feed terminals, the normalized field values at the same observation point are obtained, which will be denotes by $\mathbf{E}_N$. The main difference between these fields is that $\mathbf{E}_S$ is obtained when the feed absorption is taken into account and $\mathbf{E}_N$ is obtained without any feed absorption. The feed scattering factor γ is than defined as the ratio of the scattered field to the normalized field.

The re-radiated field, of which the magnitude can be derived with γ, can (partly) be considered as a reflection between the reflector and the feed. Figure 2.1 shows how the incident field

can be scattered by the feed and how it can re-enter the feed again after being reflected by the reflector or the support legs of the feed. Some of Morris' results were obtained by using a primary focused (single reflector) telescope model. He showed that the scattering factor γ changes by adjusting the flange width of a circular waveguide feed with plane circular flanges, where the flange width is indicated by θ_L in Figure 2.1. In a way this can be seen as changing the feed parameters by taking more or less feed scattering towards the apex of the parabolic reflector into account. Though he only considered reflections which followed path A, he suggested that with a simple extension to his approach the cases of B and C could be covered.
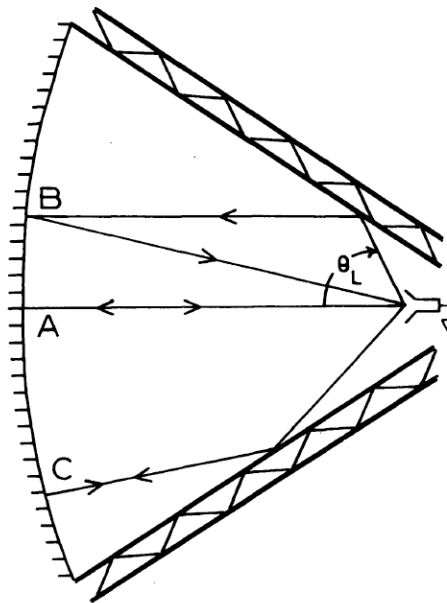

Figure 2.1: Three possible paths for the scattered energy on the feed to return into the feed again [23].

Moldsvor and Kildal presented a method to account for the multiple reflection. This method was used to optimize the performance of the dipole-disk fed resonant reflector antenna mentioned in Chapter 1. Moldsvor and Kildal have investigated the multiple reflections by introducing a feed scattering pattern, presented in [14] and [15]. This method is applied to analyze symmetrical primary-fed reflector antennas. By combining the results of the radiation pattern of the feed and its scattering pattern they introduced a method to estimate the total electric field incident on the reflector. The scattering pattern is derived through an iterative process, taking multiple reflections into account. This method (*the multiple-scattering approach*) made it possible to improved the calculation of the directivity and the radiation pattern of a symmetrical primary-fed reflector antenna, where Morris [23] presented the scattering behavior of the feed which only takes one reflections into account.

With this iterative method, they were able to estimate a very good approximation of the performance of the resonant reflector antenna. In 1988 and 1992, when Moldsvor and Kildal presented their work, it was quite difficult to calculate or simulate the performance of large

reflector antennas. Computers in those days were very limited with respect to the amount of computational power, the amount of computer memory and available simulations tools. They were able to calculate the performance of the resonant reflector antenna, which had a reflector dish with a diameter of around 6 wavelengths, because of its relative small size. These results were used to verify the results obtained with the *multiple-scattering approach*.

2.2 Numerical approaches

2.2.1 Physical optics

When Morris performed his research in 1978, computers and electromagnetic solvers were not as advanced as they are now. He therefore used a simple electromagnetic solving technique, which did not require an excessive amount of computational power and physical memory, to estimate the scattering fields. Morris used the physical optics (PO) approximation technique to estimate the scattered field caused by an incident field impinging on the feed and used these fields to derive a scattering factor. Physical optics is a more advanced technique than geometric optics (GO), but is still an approximation technique. GO can be used to approximately model the propagation of light (short wavelengths) without for instance taking wave diffraction and wave polarization features into account. The PO-approximation technique can therefore be used to analyze the behavior of (electromagnetic) waves when reflected or scattered by objects. Full-wave electromagnetic (EM) solvers on the other hand are accurate tools solving (part of) the Maxwell's equation and estimating the wave propagation and interaction with objects. Even though the PO-approximation technique is a relatively computational efficient technique, using it to solve wave interaction with large, complex objects will not lead to accurate results.

2.2.2 Method of Moments

Another numerical technique which can be used to solve EM problems with high accuracy is the Method of Moments (MoM) technique. With the MoM technique the surface currents on objects are estimated. The surface of this object is segmented into small planar patches, which is called meshing. On each patch the surface currents are estimated with the results that the current distribution over the entire surface of the object is obtained. For obtaining accurate results with the MoM technique, fine meshing is required. The EM solving tool FEKO [27] uses a minimum mesh step size of one eighth of a wavelength. With this step size is can be assured that the estimated surface currents (and fields) are in good agreement with the physical surface currents (and fields). It can therefore be evident that there is a relationship between the size of the objects, the number of unknowns (number of mesh cells) and accuracy of the results.

Kildal used this method in 1985 for estimating the reflector-feed interaction of the dipole-disk fed resonant reflector antenna. Using the MoM technique, he first analyzed and optimized the feed performance, namely the feed radiation pattern. The feed is much smaller in size than the reflector and therefore easier to solve with the MoM technique. Successively, the parabolic reflector was added to the model. Since the parabolic reflector of the antenna is larger than

the feed (diameters of six times the operational wavelength where used in [15]), estimating the surface currents on the reflector was be computationally quite extensive.

2.2.3   Hybrid techniques

Over the years other techniques were presented for analyzing the performance of the parabolic reflector antennas. Moldsvor and Kildal presented the MoM with the physical optics and uniform theory of diffraction (PO-UTD) approach, which they used to verify their *multiple-scattering approach* (presented in 1988 and 1992 in [14] [15] respectively). The MoM technique was again used for studying the feed and for estimating its radiation pattern. The PO-approximation technique was used for estimating the main beam and the near side lobe interaction on the reflector and the UTD technique for the far side lobes interaction on the reflector. Where the PO-approximation technique is limited in accurately solving EM scattering problems, the UTD technique takes the diffraction of the EM waves into account and is therefore better suited for estimating the EM wave scattering around the edges of the reflector. The EM fields reflected by the reflector, derived with the combined PO-UTD techniques, will impinge on the feed and are then scattered back by the feed. This scattered field is in a way re-radiated by the feed and are added to the previous radiated fields of the feed, such that multiple reflections can be taken into account. This technique is able to solve EM problems faster than applying the MoM technique on the complete antenna and was proven to be just as accurate [14] [15]. A big advantage of the combined MoM/PO-UTD technique is that larger models can be analyzed, since it required less computational power and storage memory.

As mentioned, simulating large reflector antennas requires a lot of computational power. The feeds which are used can sometimes be quite complex. It is therefore often preferred to first simulate the feed and to study its radiation pattern and scattering behavior. A reflector dish is much larger in size and it will not have to be simulated with the same accuracy as the feed. The reflector dish serves as a (simple) reflecting mirror, reflecting the EM waves which are impinging on it.

In 2002, Heldring has studied the possibilities of simulating electrically large structures with high accuracy [24]. He defined electrically large structures by objects, in this case the reflector dish, which have a surface area larger than $100\lambda^2$, where λ is the wavelength of the EM waves which the reflector antenna is designed for to receive. Some of the methods examined in his work are the PO-approximation technique, the MoM technique and the multi-level fast multi-pole method (MLFMM) algorithm. The PO technique cannot be used to estimate the radiation patterns of a feed, since it lacks the accurately of solving small EM problems. The MoM technique on the other hand is not suited large objects, since that would require excessive computational power. It is limited to objects with a total surface area in the order of $10 - 100\,\lambda^2[\text{m}^2]$), depending on the available computational power [24]. High accuracy comes at the cost of computational power and will at some point be limited because of the available computational resources. The MLFMM algorithm, which is an advanced method to accelerate the MoM, is a technique which is suitable for the analysis of very large EM problems and therefore very large objects. Instead of having one computational domain, the whole model is divided into smaller sub-domains. All the sub-domain uniformly filled with vacuum are

neglected, therefore creating a smaller computational domain. Objects with a surface area of $10.000\lambda^2$ can be analyzed with this technique. Just as for the MoM, the MLFMM is a full-wave method. It is therefore a more efficient technique for analyzing large objects, than the PO-approximation or the UTD techniques. Heldrings choose to use a hybrid simulation approach in his research, using the MoM and the MLFMM techniques. The combination of these two techniques resulted in a better reflector antenna performance analysis than the hybrid approach of the MoM and the PO-UTD techniques. The MoM/MLFMM hybrid technique can benefit from each separate technique, namely the high accuracy feed analysis and the possibility of analyzing a large reflector dish.

Franson [25] presented his research on a hybrid techniques by using the commercially available numerical solver FEKO [27]. Franson researched a hybrid simulation technique by analyzing an electrically large millimeter-wave antenna using the MoM-PO technique. Franson noted that the main trade-off in EM simulations is the accuracy versus the amount of physical memory and computational speed. The main dependence here is again the meshing of the object, where the electrical size (in wavelengths) is more important than the physical size. With the EM solving tool FEKO [27] he was able to perform full-wave simulations of the feed using the MoM technique and approximate ray-based calculations of the reflector dish with PO and UTD. Since again the feed analysis needs to be performed with more accuracy than the analysis of the reflector dish, the hybrid technique of MoM and PO provided a good solution. In FEKO this can be performed in two way. One way is that FEKO offers the possibility of running a hybrid MoM/PO simulation. Another possibility, with which the computational efficiency can be increased, is by importing and exporting far-field radiation patterns from one model into another. An equivalent point source from the feed far-field radiation pattern can therefore easily be imported into the complete antenna model.

One technique that is not much used for simulating reflector antennas is the finite-difference time-domain (FDTD) technique. The FDTD technique is a full-wave technique, which uses volume meshing and would therefore take all the space between the reflector and feed into account. Computationally this would require a lot of extra power and memory. This technique has therefore barely been using for simulating reflector antennas. It might prove to be a suitable technique for this research, since in this research the space between the reflector and the feed will have to be analyzed.

2.3 Applicable methods

2.3.1 Important aspects

One aim of this research is to simulate the standing wave phenomenon and confirm that the standing waves and the multiple reflections have an actual effect on the antenna performance. Until now, it has been assumed that the antenna gain fluctuation is caused by the presence of the reflections. It is therefore important that the phenomenon can be observed, that is the standing waves and the effect it has on the antenna performance. This would require an electromagnetic simulation tool that could be used to observe the space between the reflector and the feed. A grid-based simulator seems then the natural choice.

Since radio telescopes are electrically large structures, it is difficult to analyze the complete structure with a grid-based technique, since this would require a lot of computational power and storage memory. However, nowadays computers and EM simulations tools are becoming more advanced. This means that it is possible to analyze increasingly larger structures. Hybrid techniques have been developed, but they are not all available in the current commercial EM solving tools. It is therefore important to investigate what the possibilities are of simulating large reflector antennas with a commercial EM solving tool available nowadays.

The feed characteristics play an important role in the effect of the standing wave phenomenon. Measurement results obtained with the WSRT showed that the gain variations of the antenna was not observed using the FPA feed, whereas is was when the horn antenna is used. The feed analysis therefore also plays an important role in this study.

Another aspect where the absorption of the feed is important, is the frequency range of the performed measurements. Most antennas used for radio astronomy are designed to be operational over a frequency band of a few hundred megahertz. At this frequency the absorption of the feed is assumed to be at a maximum and the reflection coefficient at a minimum. For the surrounding frequencies the absorption can be assumed to be less, which will probably results in more scattering. The resonant reflector antenna presented by Kildal [13] was designed to operate at a single frequency. Therefore different absorption characteristic were not taken into account, but will be analyzed here.

Analytical studies have been performed on the multiple-reflections in reflector antennas and numerical techniques have been studied to analyze that behavior. Allen [6] and Popping and Braun [11] have developed techniques to filter the antenna gain variation out of the measurement data through data processing, which could only be done to some extent. Popping and Braun suggested that a solution for fully eliminating the effect of the standing wave phenomenon would probably require a scattering treatment of the reflector antenna to physically eliminate the multiple reflections. In the present study the feed characteristics will be analyzed in order to investigate in what way they contribute to the effect of the standing wave phenomenon.

2.3.2 EM solving tools

Several commercially available electromagnetic tools for simulating (large) reflector antennas are GRASP (General Reflector Antennas Software Package, a product of TICRA) [28], FEKO [27] and CST Microwave Studio® [29]. GRASP and FEKO are tools of which a free (student) version can be downloaded (see [28] and [27]). Unfortunately the free versions are quite limited in their functionality, only a limited number of solving techniques can be used and a maximum model size is set. GRASP, which is a numerical integral solver, offers the possibility of running simulations of electrically large structures with the use of the (advanced) PO or geometric theory of diffraction (GTD) techniques, where GTD is a prior technique of UTD which cannot be used for complex structures. It is a very easy and simple to use tool, is especially applicable for simulating (large) reflector antenna and is a reasonably fast tool. Unfortunately, GRASP does not have the possibilities of using full-wave techniques and it therefore not suited for analyzing feeds. This tool (full version) has been used at ASTRON for analyzing the WSRT. The results

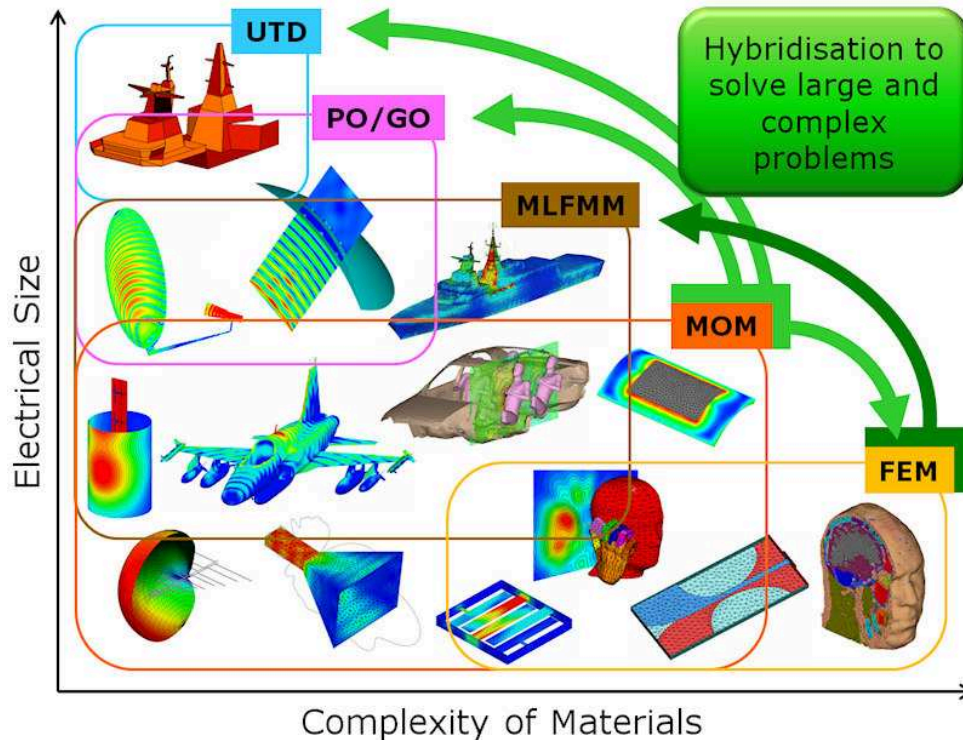obtained via GRASP were furtherly elaborated by means of MATLAB code.

Figure 2.2: Numerical solving techniques available in FEKO [27].

The finite element method (FEM) is a numerical technique which is applicable to the modeling of dielectric bodies. FEM is a volume meshing technique which is used for the efficient modeling of inhomogeneous dielectric bodies in terms of field distribution inside a volume.

Another commercial EM solving tool is FEKO. Besides the possibility of using the PO and UTD techniques, two other important techniques can also be used, namely the MoM and the MLFMM techniques. Figure 2.2 shows how these techniques are arranged with respect to electrical size and complexity of the object(s). FEKO offers more possibilities than GRASP. One important feature of FEKO is the hybridization technique, where multiple techniques can be used in one model. The MoM-PO hybridization is one of these techniques, which is ideal for simulating a complex feed with a reflector antenna. This technique can be computationally quite demanding, but will still take the coupling between different object into account just the MoM or MLFMM techniques.

CST Microwave Studio® (CST) is a specialized tool for the fast and accurate 3D EM simulation of high frequency problems and is based on the finite-difference time-domain (FDTD) technique which the other tools do not feature. Just like the MoM and the MLFMM, the FDTD is a full-wave technique. Real time domain simulations are particularly interesting if you want to study the fields propagating. However, it is also possible to obtain frequency domain results, like the S-parameters, and EM field results for many frequencies, which can be derived from one

single simulation run. The frequency domain solver of CST is more suited for analyzing electrically small structures and is therefore not of interest for this research. The integral equation (IE) solver of CST, which uses the MLFMM technique, can then again be used for electrically large structures. It is particularly useful for running radar cross section (RCS) calculations of complex objects.

Both FEKO and CST offer to opportunity of importing and exporting the (far-field) radiation patterns obtained from numerical simulations. Unfortunately, the exported data files are of a different format and cannot be easily exchanged between different tools. In CST the radiation patterns can only be imported when using the IE solver. At the TU Delft, where this work it performed, this solver is not to our disposal.

2.4 Chosen approach and modeling

For the reflector-feed interaction study, several parabolic reflector antenna models will have to be simulated and analyzed. Commercial EM solvers as GRASP, FEKO and CST can provide the results necessary for analyzing such models. Several solvers are to our disposal and different kind of results can be obtained, such as the antenna radiation pattern, the antenna gain and the scattering parameters (S-parameters). Depending on what kind of modeling has to be performed and which results we want to obtain, the right solving tool/technique has to be chosen.

One of the main obstacles, as has been discussed, is that there is a limit to the maximum (electrical) model size which can be simulated, depending on the computational power/memory and the solving technique applied. For the work of this thesis, two computers are at our disposal for performing the simulations, with the following specifications:

- 3.0 GHz Intel® Core™2 Duo processor (E8400) with 3.25 GB of RAM and Windows Professional 32-bit.

- 3.0 GHz Intel® Xeon® Core processor (5160) with 8.0 GB of RAM and Windows Professional 64-bit.

Both computers have sufficient storage memory for storing the simulation results of the reflector antenna models. The first computer can easily be used for simulating simple and small models. When the size of the model becomes too large or a very high accuracy is required, the second computer can be used. The latter will also have its limitations regarding the computational power to simulate electrically large structures.

Several important research aspects have been discussed. These aspects need to be kept in mind, when choosing the appropriate approach and simulation tool/technique for the reflector-feed interaction analysis. Beside the possibility of being able to observe and analyze the standing wave phenomenon, a feasibility study needs to be performed about the maximum model size which can be simulated. Different feeds will have to be analyzed to investigate what their effect is on the presence on the standing waves. With the measurement results of the WSRT telescope in mind, the antenna gain variation over frequency is one of the features that we want to estimate.

The WSRT telescope is a complex telescope, with its large size and different feeds. A scaled model or a simplification of it will therefore have to be analyzed.

Three different configurations will be analyzed and are shown in Figure 2.3.
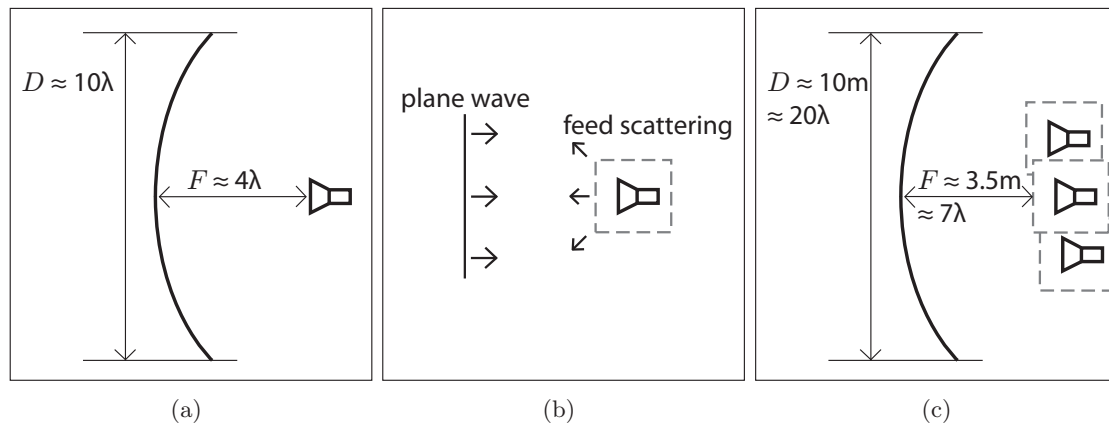

Figure 2.3: Configurations under study. (a) Reflector antenna model with feed operating at 1.695 GHz; (b) Feed study; (c) Reflector-feed simulations with feed operating at 600 MHz.

2.4.1   Experimental configuration

For the first configuration it is important to observe and study the reflector-feed interaction. For this a standard parabolic reflector antenna will be analyzed (Figure 2.3(a)). Our aim will be to simulate and study the standing wave phenomenon with this model. Kildal presented a parabolic reflector antenna in [13], of which the antenna directivity is maximized using the contributive effect of the multiple reflections between the reflector and the feed. With a focal length of four wavelengths and a diameter of about ten wavelengths, where the wavelength is 177 mm, it is relative small antenna should pose no problems with respect to the available computational resources. The published results can be used for comparison and verification of our simulation results. In Chapter 3 the parabolic reflector antenna is described in more detail and the results of the simulations are presented.

The direct observation of the standing waves will have to be performed between the reflector and the feed. GRASP and FEKO are tools which use surface current calculations to determine the radiating electric and magnetic fields. Even though the MoM, which uses surface meshing, is an effective technique when there is small surface/volume ratio, the space between the reflector and the feed can not be observed over time. The transient solver of CST, the FDTD technique, enables to observe the propagating fields. This makes the identification of the standing waves easier. From the FDTD simulations the same results (S-parameter, radiation pattern, etc) can be obtained as for the MoM simulations. This is one of the main reasons why CST is the chosen tool for carrying out these EM simulations.

2.4.2 Feed configuration

The feed analysis is part of the second configuration (Figure 2.3(b)). It is important to analyze the feed with respect to its scattering behavior and its absorption properties. Since the aim is to find a way to eliminate or mitigate the effect of the standing wave phenomenon, it is necessary to know if this can be obtained with specific feed properties. Feed analysis can be performed with both FEKO and CST and they both have the ability to export the far-field radiation pattern in case when a hybrid technique has to be applied. GRASP only has the ability of using the PO-approximation and is therefore not suited analyzing feeds.

The feeds which we will be studied will vary from the dipole-disk feed, used in configuration 1, several horn feeds and an array feed. The corrugated horn feed used for the WSRT telescopes will also be analyzed. One of these horns, the double 21/49 cm corrugated horn is shown in Figure 2.4. The FPA feed will be more difficult to simulate. First of all, it is composed out an array of element. Each element is again a Vivaldi antenna which has a refined shape. Simulating the FPA will have to performed with a very fine mesh size, which will again acquire much computational power. It would therefore be easier to simulate a more simple array. In Chapter 4 different feeds will be analyzed in order to find out what effect they will have on the reflector-feed interaction. CST and FEKO can both provide the same type of simulation results for this study. Since the dipole-disk feed is already used in the first configuration, it is already modeled in CST. Therefore, for consistency, the other feed(s) will also be modeled with it.
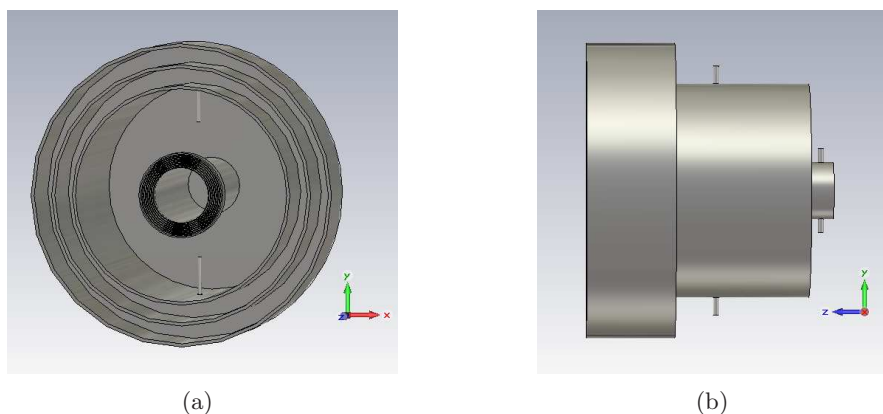

(a)	(b)

Figure 2.4: A WSRT corrugated horn feed, consisting of a 21 cm (inner) and 49 cm (outer) horn. (a) front view; (b) side view.

2.4.3 Complete configuration

The simulation and analysis of an electrically large parabolic reflector antenna will be most challenging and will be the third configuration under study. Some of the studied feeds from the second configuration will be simulated and analyzed with the presence of a parabolic reflector. The full-wave techniques (MoM, MLFMM and FDTD) which use surface or volume meshing automatically take the multiple reflections, and thus the reflector-feed interaction, into account.

An iterative approach, as used for some hybrid techniques, is therefore not needed. Large reflector antennas are unfortunately most of the time difficult to simulate, because of the fact that the electric size of the parabolic reflector is too large. All three EM solving tools have the possibility of using some sort of PO-approximation technique. Unfortunately, the IE solver of CST is currently not available at the TU Delft/IRCTR. Several hybrid techniques have been presented and analyzed. FEKO is the only tool which offers a hybrid simulation technique, but it still required a lot of computational power to solve a large model. Another possible approach would be to use the far-field radiation pattern of a feed and import it into a parabolic reflector model. Through a PO-approximation technique the radiation pattern of the parabolic reflector can be estimated. To account for the multiple reflections, this field would have to impinge on the feed again, and so on. It would be a difficult task to account for the reflector-feed interaction this way. Except the MoM-PO technique in FEKO, other hybrid technique presented earlier are seem not to be commercially available. With the computational power we have to our disposal, we will thus research the possibilities of simulating and analyzing a parabolic reflector antenna of an as large as possible size. This will therefore resemble a large radio telescope and the antenna gain will them be as large as possible. This might have an advantage to the fact that the multiple reflection cause a variation of the antenna gain. The higher the antenna gain, the better the gain variation can be observed.

The two most suitable approaches would be the transient solver of CST and the hybrid technique of FEKO. Both solvers will require a signification amount of computational power when large parabolic reflectors are simulated. A big advantages of these solvers is that the interaction between the reflector and the feed will be taken into account in one simulation run. CST has a better and more elaborate user interface when compared against FEKO. It provided some advanced post-processing algorithms and enables consistency in the use of FDTD for all the configurations under study. Further details of the third configuration model will be presented in Chapter 5

Chapter 3

Standing wave simulation

The interaction between the reflector and the feed will first be analyzed by observing the standing wave phenomenon and its effect on the antenna performance. A parabolic reflector antenna which can be used for performing these analyses will be presented in this chapter. This reflector antenna was studied in the past and previous results can therefore be used to verify our results/method. These results will give a first indication on the possibilities of simulating and analyzing a reflector antenna with the selected approach. No attention will be paid to the electrical model size limitations in this chapter. The model which will be analyzed is small enough to be simulated and later on in the Chapter 5, more attention will be paid on simulating electrically large antennas.

The actual presence of the standing waves has never directly been measured or observed. The results of this chapter should give us the confirmation that the standing waves are the actual cause of the antenna gain fluctuation. If this can be observed and proven, we might be able to find solutions for mitigating or elimination its effect.

The approach chosen in Chapter 2 will be applied in this chapter. Analysis of this approach will give a clear indication that this method can be applied to possibly larger electric size models and the possibility of obtaining the necessary results.

3.1   Reflector antenna with dipole-disk feed

The dipole-disk fed resonant reflector antenna has already been briefly described in Chapters 1 and 2. This antenna has been described and extensively studied by Kildal and Skyttemyr in [17] and later optimized in [16]. This reflector antenna consists of a parabolic reflector and a dipole-disk feed which is held in place by a tube. This tube is connected to the apex of the reflector on one end and the disk of the dipole-disk feed on the other hand and contains the wiring of the antenna feed. The dipole-disk antenna, with a beamforming ring for controlling the electric and magnetic radiation pattern, is used as a feed for the reflector antenna and is positioned at the focal point of the parabolic reflector (see Figure 3.1). The rather simple and electrically small design of this reflector antenna makes it an easy object to study. By varying the size of the

dipole-disk feed (beamforming ring, dipole or disk), slight adjustment can be made to alter the antenna performance. The position of the feed, with respect to the parabolic reflector, is also a parameter which can change the antenna performance.

The dipole-disk antenna consists of a half wavelength dipole with a plane circular disk on one side. On the other size a beamforming ring is added. From here on the dipole-disk antenna with beamforming ring will be addressed as a dipole-disk feed. The purpose of the disk is to direct the electromagnetic fields towards one direction, in this case towards the apex of the parabolic reflector. The (conducting) beamforming ring compresses the magnetic field pattern of the dipole-disk antenna whereas it has no effect on the electric field pattern. It therefore increases the aperture efficiency of the dipole-disk antenna [13] [16]. In Chapter 4 this feed will be analyzed in more detail.
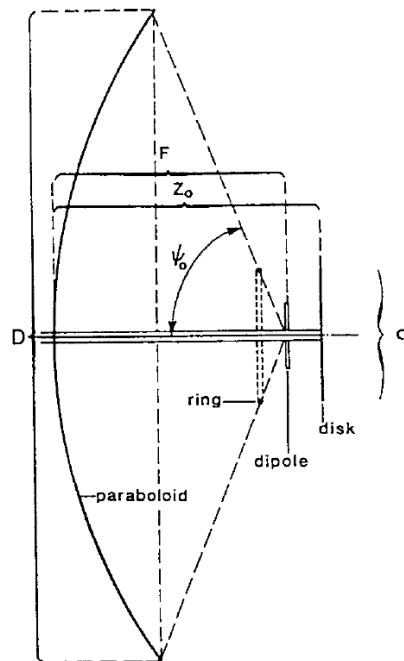
Figure 3.1: Dipole-disk fed resonant reflector antenna as presented by Kildal et al. [16].

This reflector antenna is a suitable antenna to perform our first reflector-feed interaction study on. The disk of the dipole-disk feed gives a clear indication of blocking the aperture of the parabolic reflector. The amount of blockage can be estimated by dividing the size of the disk by the aperture of the reflector. The blockage causes the electromagnetic waves to reflect on the feed, which gives us the confidence of multiple reflections being present.

The reflector-feed spacing is also of importance. Kildal and Skyttemyr showed that the feed location has an effect on the directive gain of the reflector antenna. They designed this reflector antenna to operate at a small frequency band (± 0.66 MHz) with a center frequency of 1.691 GHz. By adjusting the reflector-feed spacing, they were able to use the multiple reflections in a constructive way to obtain a maximum antenna gain. The gain obtained from these multiple

reflections was found out to almost completely compensate for the directivity loss due to the blockage of the feed. Using their results and observing the antenna gain over a frequency range should therefore give an indication on how the antenna gain would vary for the reflections of waves with different wavelengths.

Optimized dimensions of the resonant reflector antenna were presented by Kildal et al. in [16]. With the dimensions presented in Table 3.1 the directivity of the reflector antenna was optimized when operating at a frequency of 1.695 GHz and therefore at a wavelength of 177 mm. The dipole-disk spacing is a quarter of the operational wavelength, whereby the dipole is close to the focal point of the parabolic reflector.

	size in wavelength	approx. size in m/mm
Diameter of the reflector	10.3151λ	1.825 m
Disk-reflector spacing	4.3656λ	77.3 cm
Dipole-reflector spacing	4.1156λ	72.85 cm
Focal length reflector	4.1232λ	72.98 cm
Disk radius	1.1λ	20 cm
Ring location	0.4678λ	8.3 cm
Ring radius	0.5637λ	10 cm
Ring thickness	0.0169λ	3 mm

Table 3.1: Optimized dimensions of the resonant reflector antenna, where the wavelength λ is 177 mm [16].

Kildal et al. used the MoM-PO/UTD technique for obtaining their results, in our case the FDTD technique was used. Results from both simulations will be compared to verify their consistency and will give us the confidence that our approach is valid.

3.2   Model implementation

The CST model of the resonant reflector antenna used is created from the optimized dimension. The tube, which would normally hold the feed in place, is not taken into account in this model. Kildal et al. concluded that the presence of the tube has no effect on the directivity on the reflector antenna. It is therefore left out, for simplification of the model. In Figure 3.2 the CST models of the reflector antenna and the dipole-disk feed are presented. The parabolic reflector, the dipole, the beamforming ring and the disk are all perfect electric conducting (PEC) materials. The parabolic reflector is positioned in the xy-plane of the Cartesian coordinate system, with its center and focal point position along the z-axis. The dipole is positioned along the y-axis and will create an EM field which will propagate in the positive z-direction towards the reflector, since the disk is positioned behind it. The rods which connect the beamforming ring with the disk, are of a dielectric material.

All except the parabolic reflector can be created in CST from basic shapes (dipole and disk

from a cylinder and the beamforming ring from a torus). The parabolic reflector was therefore created by rotating a parabolic curve in a full rotation. The parabolic curve is described by

$$z = y^2/4F, \tag{3.1}$$

where y and z are the positions along the axes and F is the focal length of the curve along the z-axis. The rotation of a curve will apply a full circle rotation with as a results a paraboloidal object. The disk and parabolic reflector where given a thickness of 5 mm. With the FDTD technique volume meshing is applied and each object therefore needs to have a thickness. The 5 mm suffices as a minimum thickness.

(a)   (b)
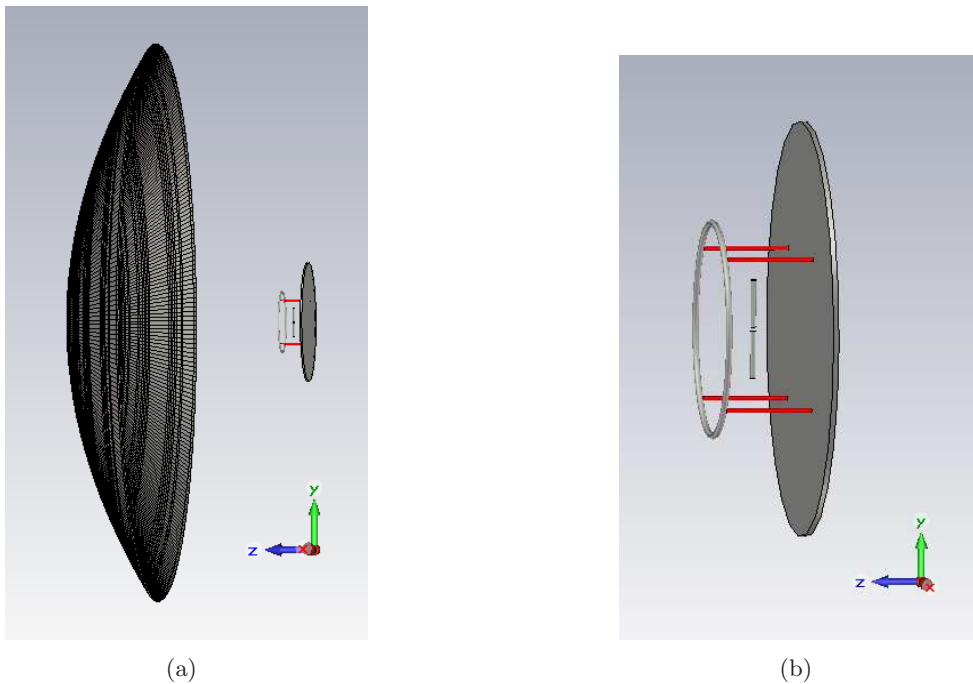
Figure 3.2: CST models of (a) complete dipole-disk fed resonant reflector antenna and (b) the dipole-disk feed.

Several possibilities of using symmetry planes, where only the half or a quarter of the model is simulated, can be applied in CST, which will reduce the simulation time and memory required. These were not used in our case. Simulations of the full model will give us the certainty that possibly asymmetric behaviors are taken into account.

The optimized dimensions were presented for a reflector antenna operating at a frequency of 1.695 GHz. The frequency analysis range for this model is set to 1.0-2.0 GHz. The already available results fall within this region and at several frequencies standing waves should occur.

To finalize the CST model, the following settings are applied. Since the reflector-feed spacing is 72.85 cm, an EM wave will has to propagate over a distance of 72.85 cm from feed to reflector. We want to observe the wave propagation in time domain and we want to observe its reflection on the feed and the reflector without the interaction of another EM field. An EM wave in vacuum

propagation at the speed of c $= 3 * 10^8$ m/s (in vacuum) and travel the 72.85 cm distance in 2.4 ns. To length of the transmitted pulse is therefore set to be between 2.4 and 4.8 ns. Other settings which are applied are the use of open boundaries, in order to guaranty that the radiation pattern (and therefore antenna gain) is calculated in the far-field region.

3.3   Simulation results

The complete model was solved in about two hours, during which the electric and magnetic fields and the far-field radiation patterns were computed. This model consist of approximately two million mesh cells. A $\lambda/10$ stepsize was applied, where λ is defined by the highest frequency of the 1.0-2.0 GHz frequency range. By defining a so-called field monitor (*E*-, *H*- or far-field), the *E*- and *H*-field results can be observed at a single frequency or over a certain time period over a specified geometrical domain. The far-fields can be specified at a single frequency or a given frequency range.

The feed radiates towards the positive *z*-direction at which point $\theta = 0°$. The *E*-plane represents the *yz*-plane ($\phi = 90°$) and the *H*-plane represents the *xz*-plane ($\phi = 0°$). The radiation patterns in the *E*-plane and *H*-plane obtained from the simulations of the reflector antenna are presented in Figures 3.3(a) and 3.4(a). The dipole-disk feed has a maximum radiation towards the positive *z*-direction ($\theta = 0°$), whereas the parabolic reflector reflects the fields towards the negative *z*-direction ($\theta = 180°$). The radiation patterns presented by Kildal et al. in [16] are shown in Figures 3.3(b) and 3.4(b). The comparison of these patterns show that with different solving techniques, the same results are obtained. In our case the maximum directivity at 1.695 GHz is 28.89 dBi, where in Kildal et al. calculated a directivity of 28.9 dBi.
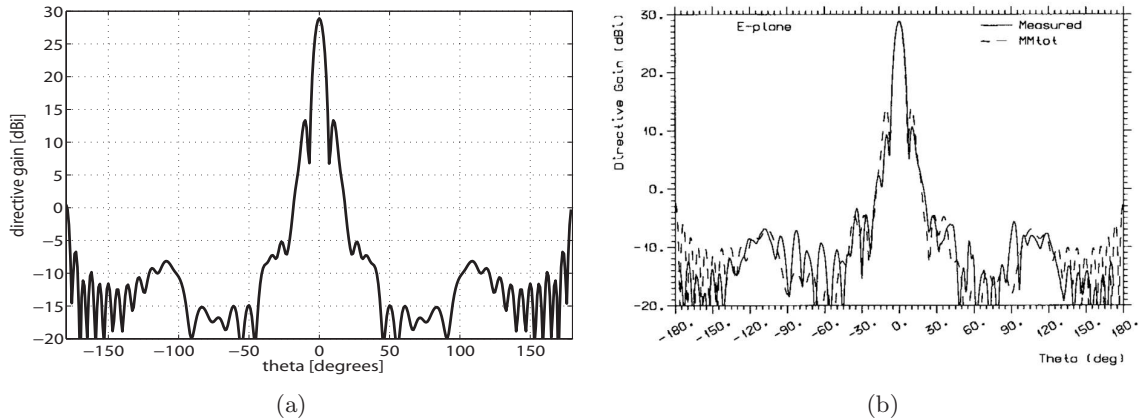

Figure 3.3: Comparison of the *E*-plane radiation patterns at a frequency of 1.695 GHz: (a) estimated pattern from CST model and (b) measured and estimated patterns from Kildal et al. [16].

Now that we have verified our results, we will analyze the reflector-feed interaction of this configuration. The two main observations we want to perform are the direct observation of the reflector-feed interaction and the varying antenna gain. For the direct observation of the reflector-feed interaction, the time domain simulations were required and will be presented in
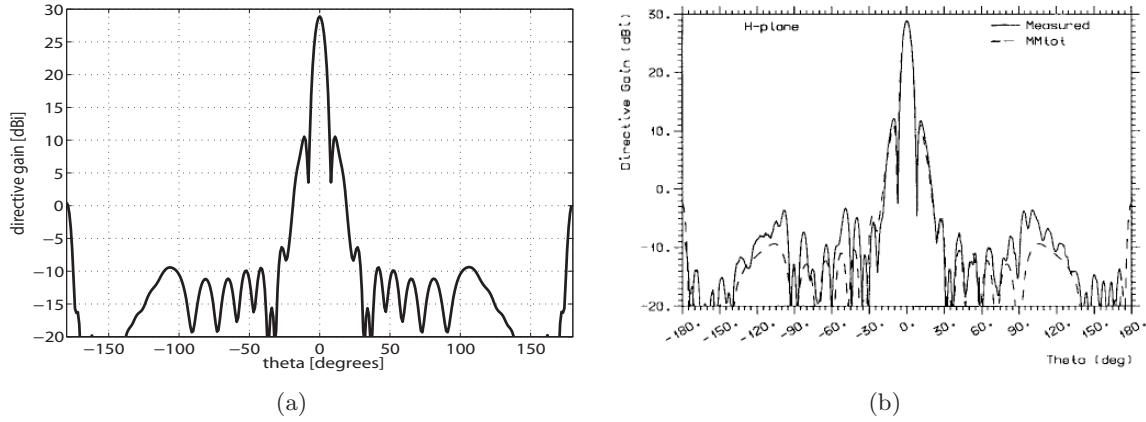
(a)   (b)

Figure 3.4: Comparison of the H-plane radiation patterns at a frequency of 1.695 GHz: (a) estimated pattern from CST model and (b) measured and estimated patterns from Kildal et al. [16].

two ways, namely the measured voltage on the (excitation) port and the electric field changing over time between reflector and feed. Direct observation of the standing waves will be analyzed by observing the phase change of the fields at several frequencies, whereas the directive gain of the antenna will be analyzed over the full frequency range.

3.3.1   Model excitation

The dipole-disk feed is excited by a Gaussian-modulated sinusoidal pulse. This pulse is generated with the center frequency of 1.5 GHz and a bandwidth of 0.5 GHz. The center frequency and bandwidth are obtained from the 1.0-2.0 GHz frequency range set for the simulations.

The dipole antenna is excited by this pulse for about 3 ns. Figure 3.5 shows this pulse which has a maximum amplitude of -1 Volt. The recorded signal at the same port has a delay of 274 ps, compared with the excitation pulse. This delay matches an EM propagating over a distance of approximately 82 mm, which is equal to twice the dipole-disk spacing. Several reflections, with a decreasing amplitude, are recorded at the discrete port and arrive at a time interval of about 5 ns after each other. The traveled distance of an EM wave is determined by

$$\text{Delay} = \text{speed of traveling wave} \times \text{distance traveled by EM wave}. \qquad (3.2)$$

The speed of a traveling wave (in vacuum) is 2.998×10^8 [m/s] and the delay $\tau = 5.02$ ns. This time delay therefore agrees with an EM wave traveling over a distance of 1.5 m. The dipole is placed 0.7285 m from the apex of the reflector (1.457 m round trip) and the disk 0.773 m (1.546 m round trip). The recorded pulses can therefore be associated with the reflections between the feed and the reflector.

No attention has been paid on studying how the amplitudes of each successive pulses decrease. With different excitation pulses or feeds the wave attenuation would differ. In this case it would not be relevant to study this, since the main goal was to indicate that the reflections can be
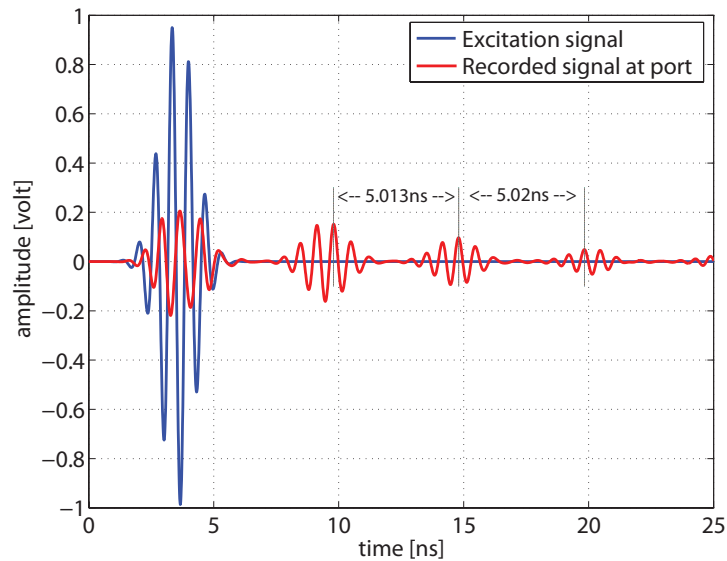
Figure 3.5: Gaussian-modulated sinusoidal pulse (blue) and measure signal at the discrete port (red).

observed.

A somewhat similar test was already performed at ASTRON. By placing a probe in the apex of the WSRT telescope (see Figure 3.6), a pulse was transmitted. In the real-time measurements they performed they were able to measure the pulse which was reflected by the feed(box). The delay between the recorded pulse (≈ 58 ns) coincided with an EM wave propagating over a distance of twice the focal length (two times 8.75 m) of the WSRT dish.

(a)   (b)
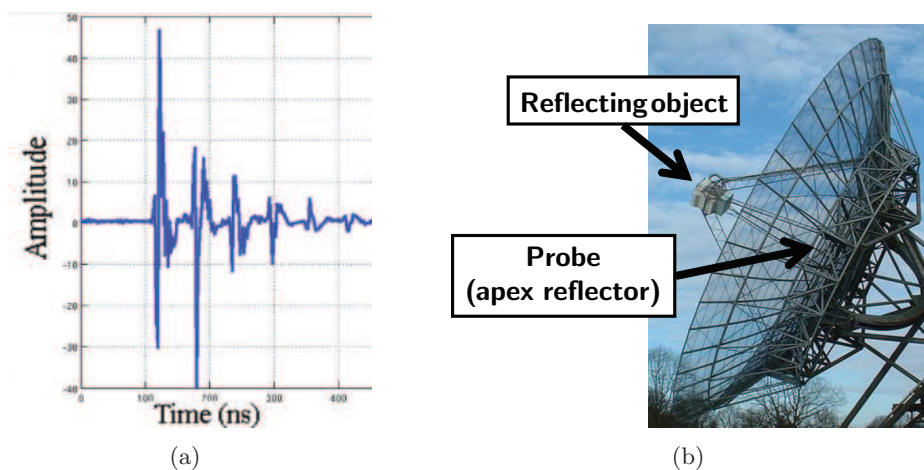
Figure 3.6: Measurement test performed of the WSRT by ASTRON with in (a) the measured signal by the probe and in (b) the test set-up.

3.3.2 Field observation in time domain

The main advantage of the FDTD simulation technique is the possibility of observing the electric and magnetic field changing over time. The fact that this requires much more computational power than for example the MoM technique does not pose a problem here. The dimension of this model are small enough for it to be solved on a standard computer. The direct observations of the propagating and reflecting fields are presented in Figures 3.7(a)-3.7(d), each at different time instants.

(a) t=3.5 ns   (b) t=5.7 ns   (c) t=7.4 ns   (d) t=8.8 ns
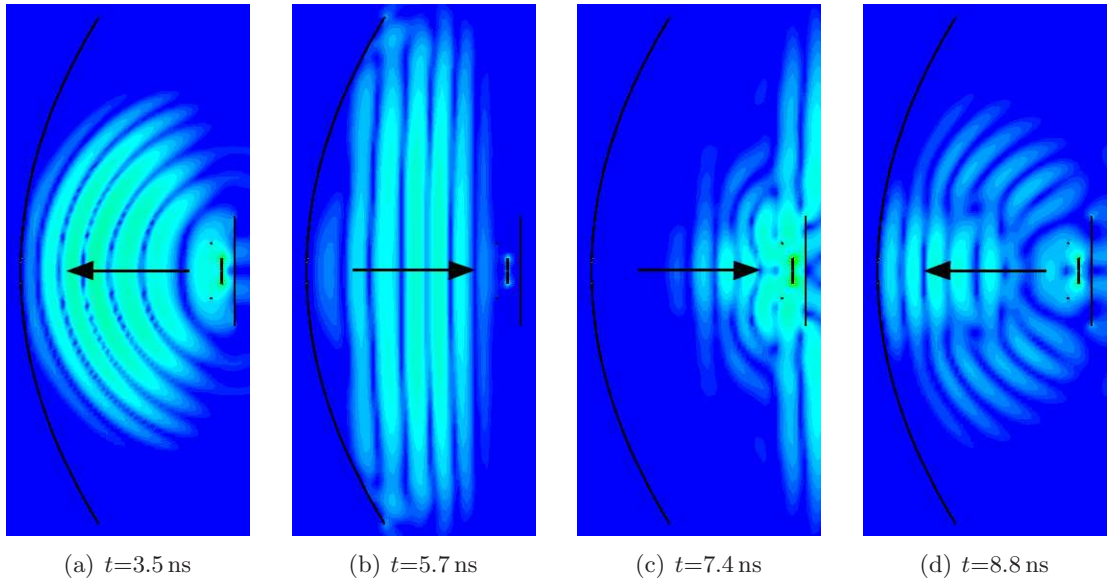
Figure 3.7: Absolute values of the E-field in the $yz-$plane propagating in the z-direction at different time samples. The black arrows show the instantaneous direction of the wave propagation.

The dipole-disk feed is excited by a Gaussian pulse and generate an E-field which propagates towards the parabolic reflector. This can be observed at time instance $t = 3.5$ ns in Figure 3.7(a). After being reflected by the parabolic reflector at $t = 5.7$ ns (see Figure 3.7(b)), the E-field propagates as a plane wave towards the feed. This E-field will partially impinge on the feed and partially propagate past it. The incident field which impinges on the feed is scattered, as can be observed in Figure 3.7(c) at $t = 7.4$ ns. After the field is reflected by the feed the first reflection propagates towards the reflector again at $t = 8.8$ ns (Figure 3.7(d)).

In previous studies ([16] [17]) these generated and reflected fields were estimated and summed up to create an overall (far-)field or radiation pattern. With the FDTD technique in CST the fields are estimated over a large enough time span to take into account a number of reflections, until the amount of energy within the simulated volume drops below a predefined threshold (-40 dB in our simulations). Every reflection will decrease in magnitude, since most of the plane wave originating from the reflector passes the feed without impinging on it. After a certain amount of iterations the reflections between the reflector and the feed will become too small with respect to the initial radiated field and will therefore not be taken into account.

3.3.3 Field observation in frequency domain

For the observation in time-harmonic regime, the electric field at two specific frequencies is studied. The first frequency is 1.6 GHz, at which standing waves are presented between the reflector an the feed. In this case the behavior of the destructive (E-)fields should be visible. The opposite case would be when the field behave in a constructive manner. At this frequency, 1.695 GHz, the dimensions of the reflector antenna were optimized for obtaining a maximum directive gain.

Observing the E-field at a single frequency can be carried out by setting an E-field monitor for the specified frequencies. For the following observations the absolute values of the E-field are presented in the yz-plane. The 1.6 GHz and the 1.695 GHz results are presented in Figures 3.8 and 3.9, respectively. By observing the amplitude of the E-field while the phase of the signal changes, the maximum field values will be analyzed. In case when standing waves are present, these maximum field values will essentially remain at the same location. At the apex of the parabolic reflector a E-field null value is present and all other nulls stay at the same point in space. The red curves in the Figures of 3.8 give a clear indication of this fact. In Figures 3.9(a)-3.9(d) the same red curves show that the null and maximum values of the E-field vary much more in place.

(a) Phase=0° (b) Phase=60° (c) Phase=120° (d) Phase=180°
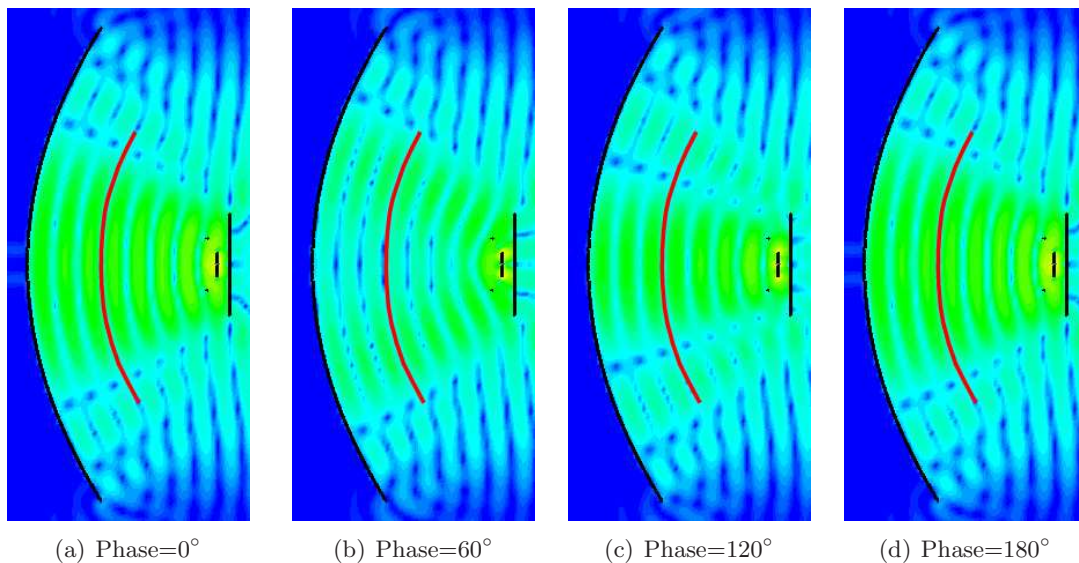
Figure 3.8: Absolute E-field values in the yz-plane at a frequency of 1.6 GHz observed at different phases, with the red curve being a figurative line representing a wavefront.

3.3.4 Far-field analysis

The final result we want to analyze, is the directive antenna gain varying over frequency. The reflector antenna presented by Kildal [13] was designed to operate over a small frequency band, while many telescopes used for radio astronomy receive signals over a wider frequency band.
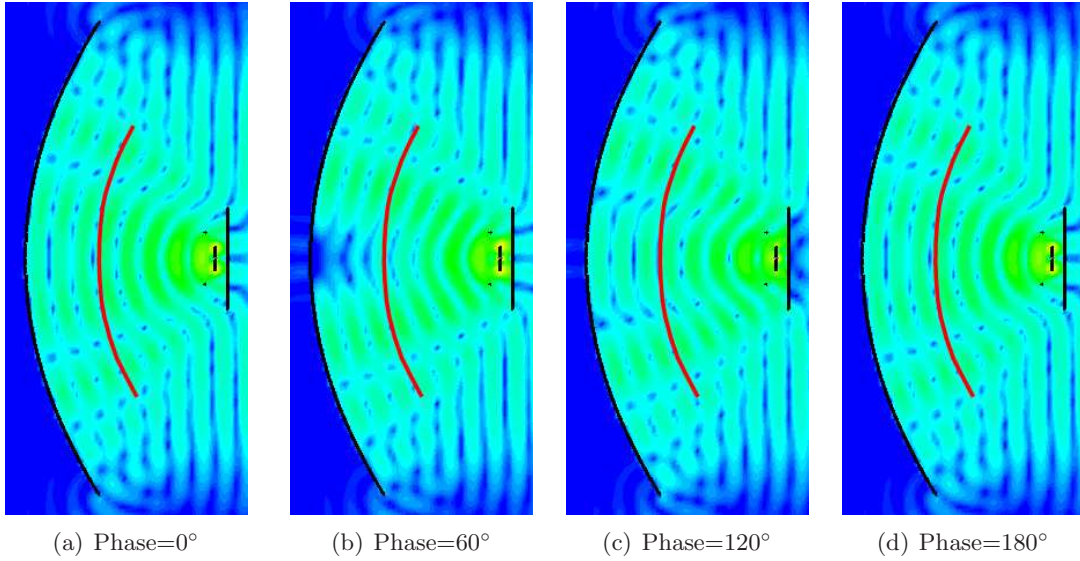
(a) Phase=0°   (b) Phase=60°   (c) Phase=120°   (d) Phase=180°

Figure 3.9: Absolute E-field values in the yz-plane at a frequency of 1.695 GHz observed at different phases, with the red curve being a figurative line representing a wavefront.

With a wider frequency band (and same antenna dimensions) the chance of encountering the standing waves phenomenon increases. It is therefore important to observe how the standing wave phenomenon effects the antenna gain. Moreover, it is our purpose to show a direct correlation between the standing waves phenomenon and the gain fluctuation versus frequency variations. This correlation was already suggested by different authors [10] [11].

The direct effect of the standing wave phenomenon can be observed by analyzing the far-field radiation pattern of the reflector antenna. In Table 3.2 the frequencies are given at which the standing waves occur.

i	wavelength	number of waves between feed/dish	frequency
1	1.5 m	1/2	200 MHz
5	0.3 m	2 1/2	1.0 GHz
6	0.25 m	3	1.2 GHz
7	0.214 m	3 1/2	1.4 GHz
8	0.188 m	4	1.6 GHz
9	0.167 m	4 1/2	1.8 GHz

Table 3.2: Frequencies where standing waves occur between the reflector and the feed, with an estimated reflector-feed spacing of 0.75 m (see Section 3.3.1).

From the far-field analysis of the CST simulation the radiation pattern of the reflector antenna can be obtained. In this case we are only interested in the maximum gain of the antenna, which points towards the negative z-direction. Results of the maximum gain over

frequency of the resonant reflector antenna is presented as the 194.7 cm disk radius line in Figure 3.10. At the specified standing wave frequencies in Table 3.2 the antenna gain drops significantly. The effect of the standing waves cause a larger drop in gain at higher frequencies, probably due to the larger electrical size of the structure at higher frequencies. The local minima appears about every 190 MHz, which is a bit smaller then the estimated 200 MHz. The disk is positioned further away from the reflector, namely 0.773 m, than the 0.75 m distance taking in Section 3.3.1 for estimating the repetition frequency ($f = c/2F$). A distance of 0.773 m can be associated with a repetition frequency of 194 MHz, which agrees better.
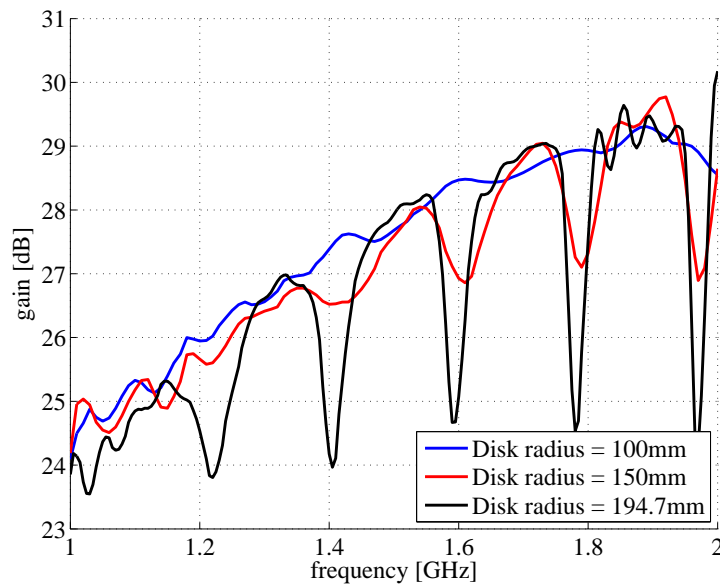
Figure 3.10: Antenna gain of the dipole-disk resonant reflector antenna, with varying dipole-disk radii.

Two other antenna gain simulations were performed and its results are also shown in Figure 3.10, where smaller radii for the disk of the dipole-disk feed are used. A smaller disk will reflect less waves, causing less multiple reflections and the antenna gain should therefore undergo less variation. With radii of 100 and 150 mm it can be observed that this is indeed the case. It must be said that the radiation characteristics of the dipole-disk feed also changes, but the disk is large enough to direct the fields towards the reflector. In the next chapter the feeds with smaller disks will be looked at more closely.

3.4 Simulation analysis

The possibility of simulating a parabolic reflector antenna has been demonstrated. The results presented in this chapter have shown that it is possible to observe the standing waves directly and that they affect the antenna variation gain over frequency. The transient solver of CST, which is based on the FDTD technique, has been applied to solve the reflector antenna model

and has proven to provide the proper results in terms of far-field radiation patterns. The direct observations in Sections 3.3.2 and 3.3.3 have shown the behavior of the reflector-feed interaction.

This chapter givea a good foundation for further analysis of the reflector-feed interaction, where different feeds and larger models will be studied. It has been demonstrated in Sections 3.3.4 that changing the feed dimension has a direct effect on the antenna performance.

To conclude this chapter, the transient solver of CST is an effective tool and will be used for the simulations of the different feeds and the reflector-feed analysis. The simulation results are reliable, since they were compared with those presented by Kildal et al. in [16]. It can now be said with certainty that the standing waves cause the gain fluctuations observed in [10] and [11].

Chapter 4

Feed study

The characteristics of a feed can have a big influence on the reflector-feed interaction. The scattering or absorbing properties of the feed are particularly of interest. A good example are the horn and the FPA feed of the WSRT. These feeds seem to behave differently with respect to the standing wave phenomenon, as was observed in Figure 1.5. By studying different feeds and analyzing their effect on the (fluctuating) antenna gain of a parabolic reflector antenna we will investigate if their is a relationship between the feed characteristics and the gain fluctuation versus frequency.

In [13], [16] and [17] different disk sizes of the dipole-disk feed were analyzed for optimizing the performance of a parabolic reflector antenna. Since the feed blocks part of the aperture of the parabolic reflector, its size is an important factor which influences to the amount of reflected incident field. A larger feed would therefore reflect more energy. The effect of these multiple reflections on the antenna gain can be observed in Figure 3.10.

The importance of the absorption of a feed has been mentioned and treated by Morris in [23]. The reflection coefficient or scattering factor of a feed determines the amount of energy which is reflected and that subsequently causes the multiple reflections. Simulations performed by van Cappellen at ASTRON have already shown that the EM field scattered on the FPA is quite small[32]. By determining the radar cross section (RCS) of a feed, this scattering behavior of a feed can be analyzed. By illuminating the feed with a plane wave, the reflected fields over different angles are determined to obtain the RCS of the feed. The RCS for a metal object in the form of a flat plate or a disk, on which a plane wave impinges, can be easily estimate by means of Equation 4.1.

$$\sigma = \frac{4\pi A^2}{\lambda^2} \, [\text{dBsm}]. \tag{4.1}$$

From Equation 4.1 it can be observed that the RCS σ is dependent on the surface area A and the wavelength λ of the impinging wave. The RCS is measured in decibel squared meter (dBsm) and gives an indication of the scattering properties of an object to represent the magnitude of the reflected incident field with respect to the incident field itself. For objects with a different shape, for example a thin wire, it is more difficult to estimate the radar cross section, since they scatter the energy in multiple directions [31]. In most cases the RCS is evaluated experientially

or numerically by means of EM analysis tools.

In general the RCS of an antenna differs from the RCS of a flat object. In [31] the RCS of a long tin wire was analyzed. Here it is addressed that part of the incident electromagnetic wave couples onto the wire. Depending on the impedance of the wire, this EM wave is re-radiated again. Therefore the RCS of a feed is not only determined by the scattering, but also by the re-radiation of the feed itself, depending on the antenna termination conditions. For the dipole-disk feed we will therefore study the feed when it is terminated by different load (matched load, short- or open-circuit termination).

In this chapter several feeds will be analyzed, of which some will be simulated with the presence of an electrically large parabolic reflector (Chapter 5). The dipole-disk feed which is already analyzed in the previous chapter will be the first feed to be studied, followed by a horn and array feed.

Besides the 1.695 GHz dipole-disk feed, an enlarged dipole-disk feed operating at a center frequency of 600 MHz will be simulated. The 600 MHz operating frequency is chosen for several reasons. First of all, it is the same frequencies the 49 cm wavelength receiver, a corrugated horn, of the WSRT which operates at (560-610 MHz). A model of this horn will be analyzed and the 600 MHz dipole-disk feed will therefore be useful as a comparison. The second reason why a center frequency of 600 MHz is selected, is because later the analysis of these feeds simulations with a parabolic reflector will be performed. We aim at simulating an electrically large reflector antenna. Since the parabolic reflector will be meshed with a stepsize of $\lambda/10$, its electrical size will be wavelength dependent. As will be made clear in Chapter 5, a wavelength of around 0.5 m (at 600 MHz) would suffice.

A conical horn feed model will be created, to represent the corrugated horn feed (49 cm receiver). Inside this corrugated horn feed a smaller horn (21 cm receiver) is present. A simpler horn design, which will have the same radiation pattern will therefore be used.

The WSRT feeds are surrounded by a feedbox, containing receiving electronics, cooling system and other instruments. This feedbox has a size of approximately 1.1 m by 1.1 m and blocks part of the parabolic reflector aperture. The feedbox has a surface area of $1.21\,\text{m}^2$ (on the side towards the reflector) and the reflector has a projected surface area of $\pi R^2 \approx 490\,\text{m}^2$, which lead to a blockage of 0.25%. In our horn simulations we will also taken the feedbox into account. An extra surface area around the horn will account for more reflections of the feed. By placing absorbing material on the feedbox, which will surroud the aperture of the horn, we will observe how the feed characteristics (RCS, radiation patterns) will change and what effect this will have on the overall antenna gain.

The frequency band applied for the simulations is 400-800 MHz. We will adopt the F/D-ratio (focal length-reflector diameter) of the WSRT telescope, which is 0.35. Simulations of a parabolic reflector with a diameter of 10 m approach the limitation of solving a reflector antenna. The focal length for such a model is 3.5 m. With wavelength varying from 0.375 m (at 800 MHz) and 0.75 m (at 400 MHz), we can be assured that standing waves will occur at multiple frequencies. With a focal length F of 3.5 m, a standing wave will occur every 42.9 MHz ($\Delta f = c/(2F)$).

4.1 Dipole-disk feed

4.1.1 1.695 GHz dipole-disk

The first analysis is performed of the dipole-disk feed described in the previous chapter. The disk radius of the dipole-disk feed has been varied to observe how the antenna gain of the reflector antenna would change over frequency. Simulations were performed where a 100 mm, a 150 mm and a 194.7 mm disk radius was used. To get an indication on what the radar cross sections of these feeds is, the RCS of each feed at a frequency of 1.695 GHz is presented in Figure 4.1. The scattering of each feed is shown over a theta angle of 180° in the E-plane. In this configuration the feed is illuminated by a plane wave with an E-field orientation parallel to y-axis and propagating in the negative z-direction. The maximum RCS appears at $\theta = 0°$, whereas at the $\theta = \pm 90°$ angles the RCS is below -40 dBsm. It can be observed that smaller disks produce less backscattering. This is expected, since the RCS is surface area dependent.
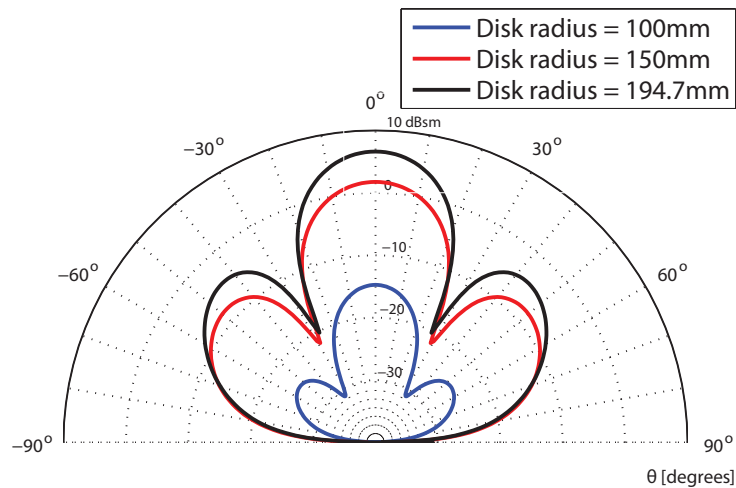
Figure 4.1: The RCS pattern of the 1.695 GHz dipole-disk feeds for different disk radii in the E-plane ($\theta = \pm 90^{circ}$, $\phi = 90°$).

The internal impedance of the voltage generator used to excite these feeds is set to 50 Ω. The $|S_{11}|$ parameter results of these feeds are presented in Figure 4.2. $|S_{11}|$ is at a minimum for all feeds at approximately 1.2 GHz. In case an incident field would impinge on the feed and the dipole-disk port is terminated with the voltage generator with a 50 Ω internal impedance (the imaginary part of the impedance, the reactance, cannot be set for a discrete port), we would expect the absorption of the feed to be maximum at approximately 1.2 GHz. At this frequency the coupling between the impinging EM wave and the dipole-disk feed is the highest. The dipole has a relatively larger impact on the RCS and causes the minimum RCS to shift over frequency.

For obtaining the RCS of each feed, the feeds are illuminated by a plane wave. At a frequency of approximately 1.2 GHz the dipole-disk feed with a disk radius of 194.7 mm shows the highest absorption over the 1-2 GHz frequency band. This is not the case for the dipole-disk feed with
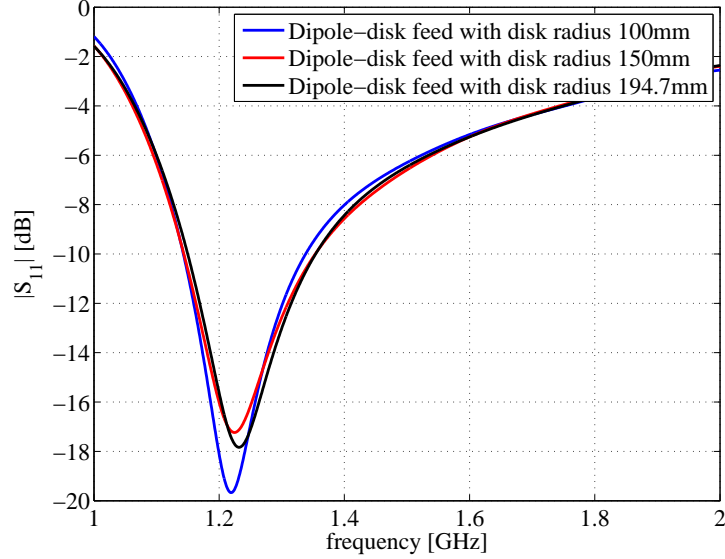
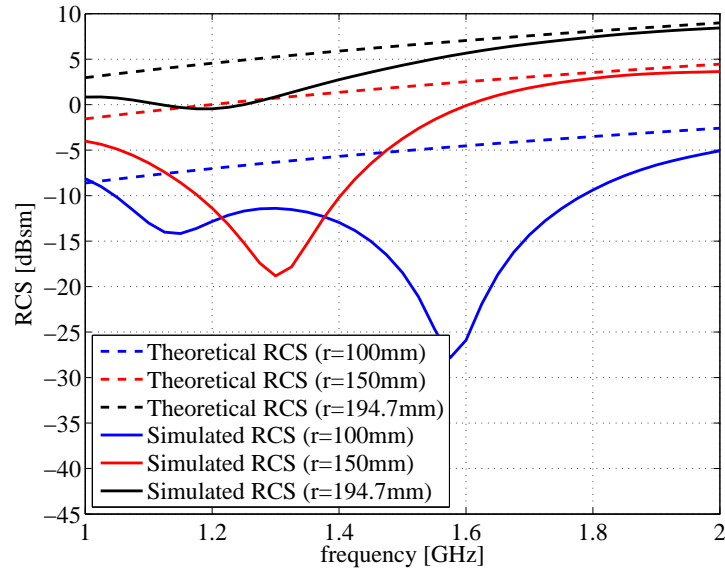Figure 4.2: $|S_{11}|$ parameters over frequency of the different dipole-disk feeds.

Figure 4.3: RCS over frequency at $\theta = 0°$ for different dipole-disk feeds.

100 mm and 150 mm radii, as can be observed in Figure 4.3. In this figure the RCS results of all three feed are presented, where the RCS values are taken in the direction $\theta = 0°$ (opposite direction of approaching plane wave). The estimated RCS over frequency of the metal disks with the same radii are also presented. The simulated results show that each dipole-disk feed has a minimum RCS at different frequencies. The presence of the dipole compared to the size of the disk plays a bigger role when the disk size decreases. Smaller disks have a lower RCS, but also a minimum RCS at a different frequency. Instead of a maximum absorption at approximately

1.2 GHz, it shifts to a higher frequency. The dipole-disk feeds do not only absorb the incident field, but start to re-radiate it. In the next section we will perform different port terminations to study the change of RCS over frequency further.

4.1.2   600 MHz dipole-disk

The 1.695 GHz dipole-disk feed was used for simulations with the reflector antenna presented in Chapter 3. In this section we will analyze a larger dipole-disk feed, where instead of the 177 mm wavelength, a wavelength of 0.5 m (at a frequency of 600 MHz) is applied. This dipole-disk feed model is presented in Figure 4.4. Dimension of this feed are (rounded values): dipole length = 0.25 m (half wavelength), dipole thickness = 2.5 mm, disk radius = 0.5 m (λ), disk thickness = 5 mm, ring radius = 0.3 m (0.6λ), ring thickness = 17.5 m (0.035λ), disk-dipole spacing = 0.15 m (0.3λ), ring-dipole spacing = 0.1 m (0.2λ), rod thickness = 5 mm (0.01λ).
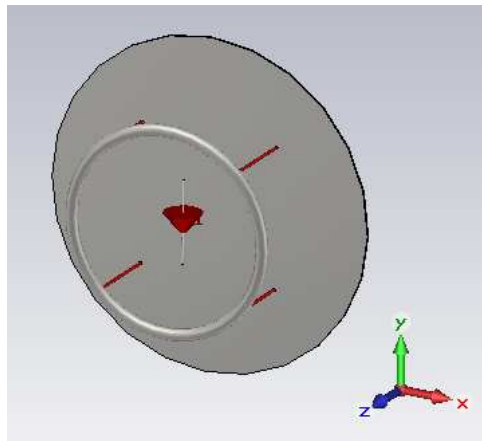
Figure 4.4: 600 MHz dipole-disk feed CST model.

This feed model will be used for simulations with an electrically large parabolic reflector and its operating frequency will be 600 MHz. For a good absorption at this frequency, we will determine the antenna impedance (Z_A) at 600 MHz and terminate the dipole-disk port with an element which is set to the complex conjugate of Z_A. The antenna impedance can be defined by the resistance (R_A) and reactance (X_A) as shown in Figure 4.5. We have first run a simulation where the feed is excited by a voltage generator (Figures 4.5(a) and 4.5(b)). From these simulation the resistance and reactance of the dipole-disk feed over frequency are obtained (Figure 4.6).

At a frequency of 600 MHz, the antenna impedance is $Z_A = 149.6 + j22.56 \, \Omega$. To confirm that the $|S_{11}|$ at 600 MHz, the internal resistance of voltage generator is set the 149 Ω (no reactance, since this cannot be specified). As is shown in Figure 4.7, the minimum $|S_{11}|$ value is around 600 MHz.

Now that we have determined the antenna impedance of the dipole-disk feed at 600 MHz, we are able to terminate the dipole-disk port with a matched load at this frequency. The
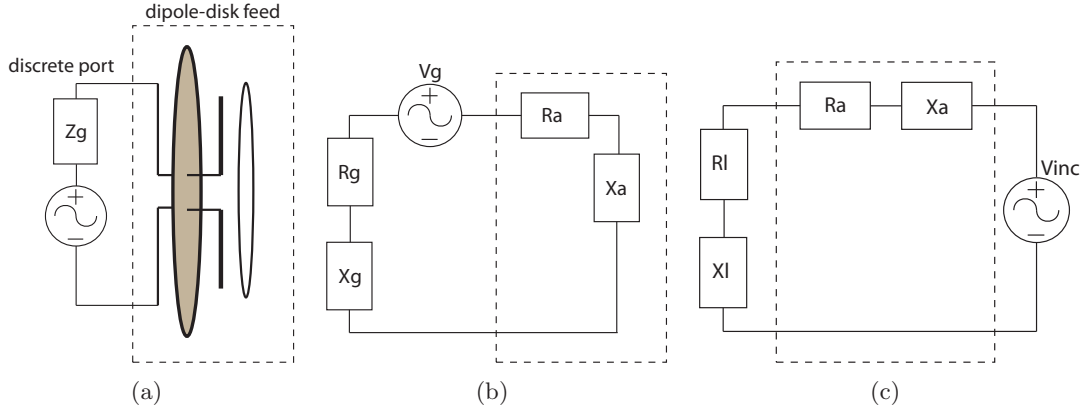
Figure 4.5: Impedance models of dipole-disk feed configurations with (a) dipole-disk model fed by discrete port, (b) electric scheme of discrete port excitation and (c) electric scheme of plane wave excitation.
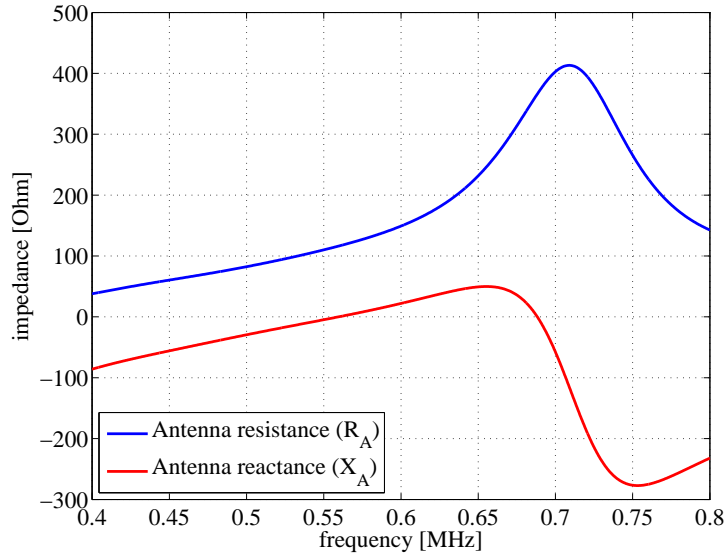

Figure 4.6: Antenna impedance of the dipole-disk feed.

following simulations, where we will determine the RCS, will be different with respect to the (voltage) source. Instead of a voltage generator, we will have an incident plane wave V_{inc} (see Figure 4.5(c)). To compare the RCS of a dipole-disk feed, which is terminated by a matched load at 600 MHz, we have also simulated the feed with a short-circuit and open-circuit port termination. The inductance and the capacitance of a port termination with a matched load can be determined by

$$Z_l = R_l + jwL_l + \frac{1}{jwC_l} = R_l + j2\pi f L_l - j\frac{1}{2\pi f C_l} \ [\Omega] \tag{4.2}$$

To match the dipole-disk port to the antenna impedance at 600 MHz, the complex conjugate
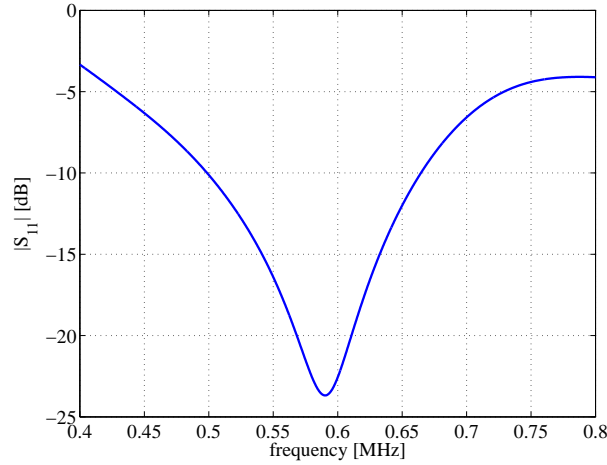
Figure 4.7: $|S_{11}|$ parameter of the dipole-disk feed at $600\,\mathrm{MHz}$ (with matched load).

of Z_A is taken as termination load. Therefore $Z_l = 149.6 - \mathrm{j}22.56\,\Omega$ and at a frequency of $600\,\mathrm{MHz}$ the capacitance is $C = 11.76\,\mathrm{pF}$. For the short circuit simulation an ideal electrical connection is used, whereas for the open-circuit termination the port will be left open.

In Figure 4.8 the estimated RCS of a metal disk and the simulated RCS results of the dipole-disk feeds with different port termination are compared. It can be observed that the RCS results of the matched load termination is alway smaller than the open-circuit port termination results, due to the absorption of the feed. At a frequency of $600\,\mathrm{MHz}$ the matched load termination should absorb most of the incident field. The RCS at this frequency does not show a drop. Part of the incident is not only absorbed, but also reflected on the disk and ring. Simulation of a dipole with a matched port termination at $600\,\mathrm{MHz}$, presented in Appendix B, has shown that the incident field impinging on it is reflected in all direction of θ for $\phi = 0°$. Therefore combining the scattering behavior of the feed and the disk, where in this case the dipole-disk spacing is $0.15\,\mathrm{m}$, will lead to a lower RCS at frequencies near 400 and $750\,\mathrm{MHz}$.

The RCS for the short-circuit port termination drop significantly at $480\,\mathrm{MHz}$. One cause of this is that less of the incident field is reflected back in the opposite direction on the incident field and more towards another direction. This can be observed in Figures 4.9(a) and 4.9(b), where the RCS patterns of the short-circuit dipole-disk termination are presented at a frequency of $480\,\mathrm{MHz}$ and $600\,\mathrm{MHz}$. The distance between the dipole and the disk for this configuration is $0.15\,\mathrm{cm}$. Since at a frequency of $480\,\mathrm{MHz}$, an EM wave has a wavelength of $62.5\,\mathrm{cm}$ (close to $60\,\mathrm{cm}$), the scattered field of the dipole together with the reflected field of the disk interfere with each other in a way that the RCS (towards $\theta = 0°$) drops to a minimum. Since the for the $600\,\mathrm{MHz}$ matched load termination most of the incident field is absorbed, this interfering behavior has less effect on the RCS.

The 3-dimensional RCS results are presented in Figure 4.9 at a frequency of $480\,\mathrm{MHz}$ (Figure 4.9(a)) and $600\,\mathrm{MHz}$ (Figure 4.9(b)). From these figures the difference of the RCS patterns can be observed and show that at $480\,\mathrm{MHz}$ the RCS is stronger to the direction other then $\theta = 0°$. In case of the $600\,\mathrm{MHz}$ RCS pattern the maximum RCS does appear at $\theta = 0°$. These
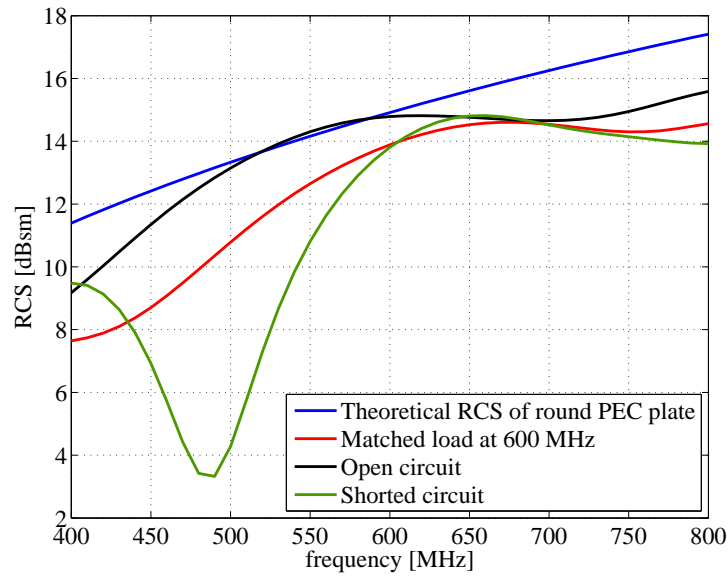
Figure 4.8: RCS over frequency in the negative z-direction ($\theta = 0°$) of the dipole-disk feed for different port terminations.

observation therefore explain the large drop in RCS at 480 MHz for the short circuit simulation results.
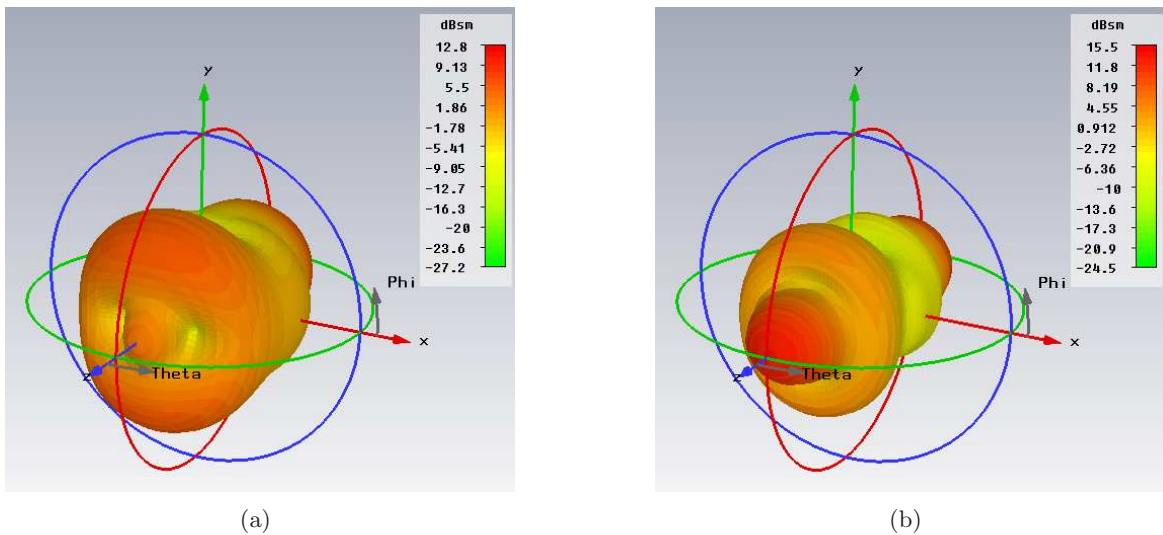

Figure 4.9: RCS results of the dipole-disk feed with short-circuit termination at (a) 480 MHz and (b) 600 MHz.

A clear relation between the RCS and frequency for the dipole-disk feed is difficult to observe, due to the absorbing behavior of the feed. The presented RCS results are obtained at an angle of $\theta = 0°$, or the negative z-direction, since we assume that most energy backscattered by the

feed is directed towards that direction.

4.2   Horn feed

The conical horn model is created for these simulations (see Figure 4.10). The aperture of the horn has a diameter of 0.5 m (one wavelength at 600 MHz). The length of the horn is also 0.5 m, whereas the length of the cylinder is 0.25 m. The flare angle of the horn is 26.8°. At a reflector edge illumination angle of $\theta = 71°$ ($\phi = 0°$) the normalized directivity of the horn is -13 dB, which is the same edge illuminations of the WSRT for the corrugated horn feed. The horn is fed by waveguide port of which the cut-off frequency for the different propagating modes is determined by the radius of the circular cylindrical waveguide. To determine the cut-off frequency of a circular cylindrical waveguide we use

$$k_{c,nm} = \frac{p'_{nm}}{a} \tag{4.3}$$

from [33]. This can be rewritten as

$$f_c = \frac{p'_{11}c}{2\pi a}. \tag{4.4}$$
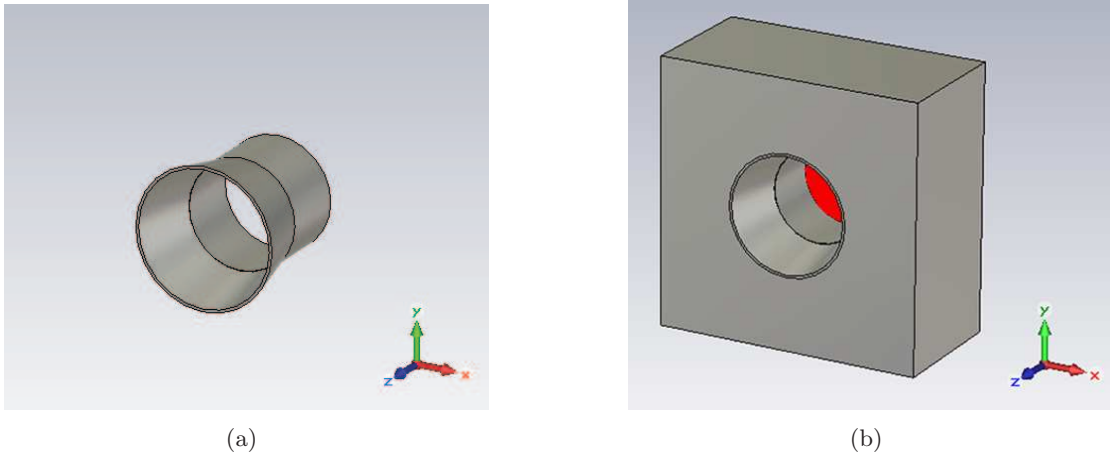
Figure 4.10: Conical horn model in (a) and surrounded by a feedbox in (b).

The cut-off wavenumber $k_{c,nm}$ is equal to $(2\pi f_c)/c$, where f_c is the cut-off frequency and c the speed of light in vacuum. a is the diameter of the circular cylindrical waveguide. The number of cyclic variation n and the root number of the Bessel function m are 1, since the preferable mode of propagation is the TE_{11} mode. From Table 5.3 in [33], a values of 1.841 for p'_{11} is obtained. For a radius of 0.2 m, the cut-off frequency of a cylinder with a radius of 0.2 m is therefore 439.5 MHz. From the CST simulation a cut-off frequency of 457 MHz was estimated, which is in good agreement with the calculated frequency.

For the TE_{21} mode, $p'_{21} = 3.054$ and the cut-off frequency is 729 MHz. The frequency range for the following simulations is therefore set from 500 to 700 MHz. This range is still wide enough for observing standing waves in the reflector-feed simulations, as it was elaborated in the beginning of this chapter.

The second and third propagating modes obtained from the CST simulations are the TM_{11} mode having a cut-off frequency of 457 MHz and the TM_{01} mode having a cut-off frequency of 596.7 MHz.

(a)   (b)   (c)   (d)
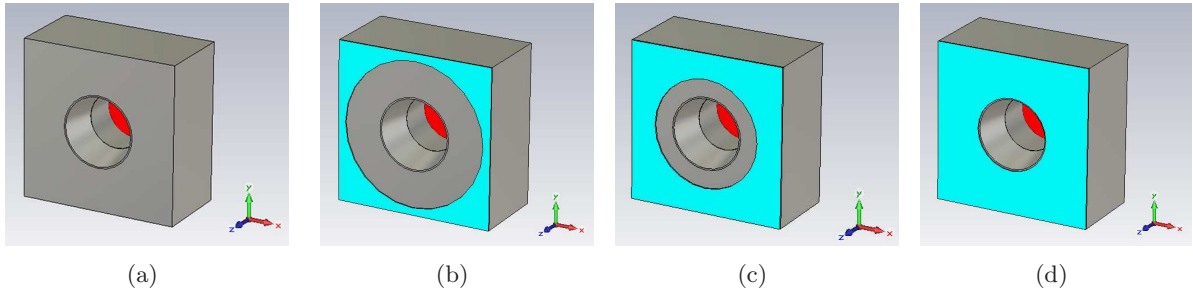
Figure 4.11: Conical horn with feedbox in (a) and with a small (b), medium (c) and large (d) size absorbing plate.

For this feed configuration the horn is surrounded by a feedbox (Figure 4.11(a)). Our aim is to change the RCS of this feed by placing an absorbing material on the surface of the feedbox around the horn aperture. The incident field would therefore be absorbed, instead of reflected. Three different size absorbers were used and each model is presented in Figure 4.11.

Since a waveguide port is used for exciting the horn feed, the port impedance is automatically matched for all frequencies. As can be observed in Figure 4.12, the $|\text{S}_{11}|$ values (of the horn feed without an absorber) are low for the 500-700 MHz frequency range. The $|\text{S}_{11}|$ values are equal for the configurations with or without the absorbers.

4.2.1 Absorbers

Popping and Braun have mentioned in [11] that the use of absorbers can cause the antenna noise temperature to rise. Since some of the WSRT receivers are cooled to below 20 K, thermal noise will affect the measurements and should therefore be avoided. In these simulations the absorbers are only used for changing the feed characteristics and can therefore not be conceived as a practical solution for eliminating or mitigating the effect of the multiple reflections.

CST provides the possibility of using the ECCOSORB® FGMU-125 material. This material is a broadband absorber with average reflectivity of -12dB over a 2-12 GHz frequency range [30]. There is no other broadband absorbing material in the CST database which is specified for absorption below 1 GHz. Simulation of the FGMU-125 material showed that in the 500-700 MHz frequency range, with a thickness of 8.5 mm and backed by a PEC plate, the reflectivity is at a minimum compared to the reflectivity of a metal plate. These simulation results are presented in Appendix C.
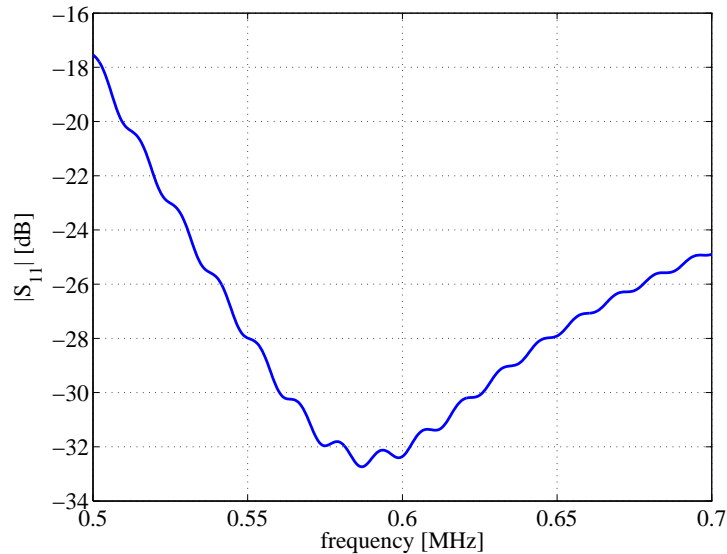
Figure 4.12: $|S_{11}|$ parameter of the horn feed.

Three different absorbing plates are used in the following simulations, each of different size. All of them cover the front surface of the feedbox, but have a different sized opening, varying from a radius of 0.25 m (large absorber) to 0.375 m (medium absorber) and 0.5 m (small absorber). The large absorber covers the whole surface area of the feedbox surrounding the aperture of the horn.

All of these feeds models will be used for simulation with a parabolic reflector, to determine the directive antenna gain. To be sure that the radiation pattern of the feeds are not affected by the presence of the absorbers, Figure 4.13 is presented. A comparison of the radiation patterns of a horn, horn surrounded by a feedbox and the absorber feed configurations are shown. The maximum gain at $\theta = 0\circ$ and the edge illumination of the parabolic reflector at $\theta = 71°$ only varies a few decibels (see Figure 4.14). These results are close enough to each other, not to cause significant changes in the antenna directivity.

4.2.2   RCS results

The RCS results are obtained in the same manner as for the dipole-disk feed, a plane wave illumination and the RCS in the direction $\theta = 0°$. For comparison, the estimated and simulated RCS values of a 1.1 m by 1.1 m PEC plate are presented together with the simulated RCS values of the horn feeds and absorbing plate in Figure 4.15. With these results we can observe the different scattering behavior of feeds with the same type of excitation, the same surface area and radiation patterns which vary very little.

To verify the correctness of this approach, the estimated and simulated RCS results for the PEC plate are presented in Figure 4.15. Since these results show almost no difference, we can assumed that they are valid. The RCS results of the horn feed model (without absorber)
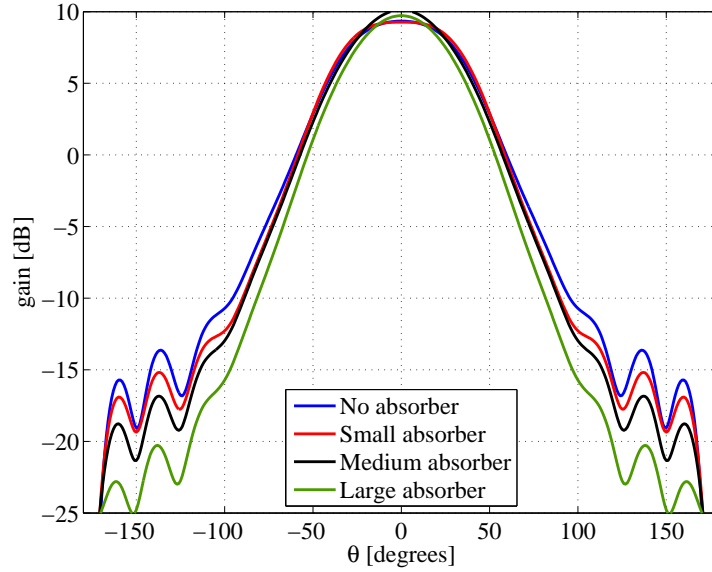
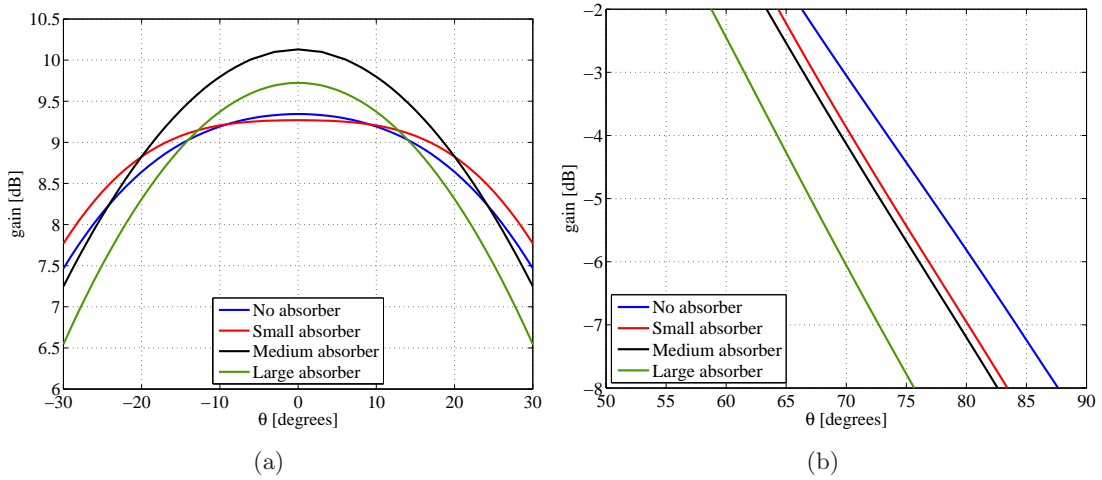Figure 4.13: Radiation patterns of different feeds in the E-plane at 600 MHz.

(a)

(b)

Figure 4.14: Different in radiation pattern focused in the maximum at $\theta = 0°$ (a) and at the reflector edge illumination angle, $\theta = 71°$ (b).

are approximately 1 dBsm smaller over the 500-700 MHz frequency range. The aperture of the horn and the waveguide port are most likely to cause this decrease in RCS. Around 600 MHz the difference is even a little less than 1 dBsm. At this frequency the horn reflects part of the incident field as was the case for the dipole-disk feeds.

The absorber simulations show a much larger drop in RCS. Three different absorber size are taken and are displayed in Figure 4.11. Each absorber differs in the radius of the opening in the middle points of the horn aperture. The surface area the absorbers cover, are from small to large $(1.1^2 - \pi r^2 \, [\text{m}^2])$: $0.425 \, \text{m}^2$, $0.768 \, \text{m}^2$ and $1.014 \, \text{m}^2$, corresponding to a surface coverage
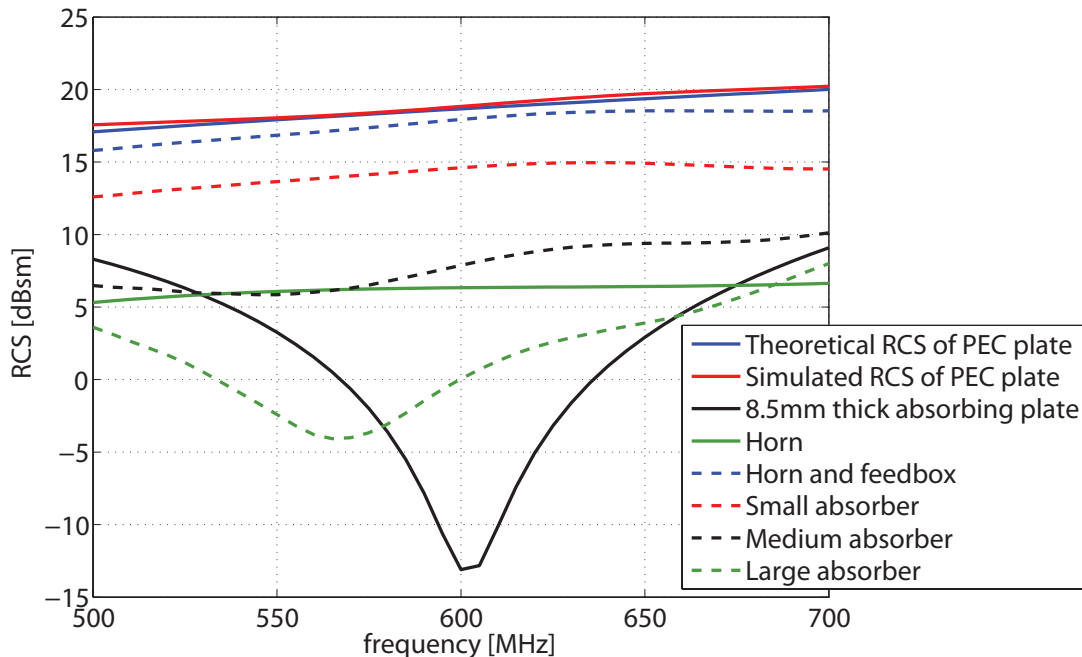
Figure 4.15: RCS results of a PEC plate and different feeds ($\theta = 0°$).

of 35.1%, 63.5% and 83.8%, respectively. For an increase in the absorber size, the RCS values approach the same level (at an angle of $\theta = 0°$) of the plate covered with the absorber.

4.3 Dipole-disk array feed

The feeds analyzed so far consists only out of one radiating element. The main difference between the horn and the FPA feed of the WSRT is the number of antennas. Since the FPA consists of multiple receiving elements, we conjecture that an incident plane wave is better absorbed and less of it is reflected than in case of the horn feed. In [32], van Cappellen has shown that the overall RCS of the FPA (presented as a Phased Array Feed or PAF) is much lower than the RCS of a plate or dipole array, especially in the direction towards the center of the reflector dish. The FPA, plate and dipole array have in these cases the same surface size on which the incident field impinges.

In the previous section we have demonstrated that the RCS of a horn feed can be reduced by placing absorbing material around the horn aperture. In this section we will analyze an array which consists of five dipole-disk antennas as feed. The complex structure of the FPA makes it a difficult object to analyze and it will take quite some computational power to simulate it because of its complexity. Due to the limited computational resources at our disposal, rather than simulating the FPA actually used at ASTRON we have chosen to analyze the dipole-disk array feed. With this simpler array we should be able to simulating the same increase of absorbing effect observed for the FPA.

4.3.1 Model set-up

The dipole-disk array model consists of five dipoles, five beamforming rings and a PEC plate, as shown in Figure 4.16. Instead of the disk, one PEC plate is placed behind all the dipoles with a dipole-disk spacing of 0.15 m, which was also used for the 600 MHz dipole-disk feed. The plate has a size of 1.1 m by 1.1 m, which gives it the same surface area (on the side of the horn aperture) as the horn feeds previously considered.
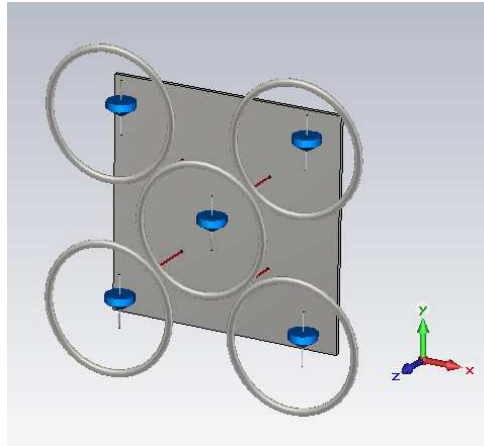

Figure 4.16: CST model of dipole-disk array feed.

The antenna impedance at 600 MHz for the dipole-disk feed was $149 + j22\,\Omega$. For this simulation, the dipoles are terminated with a load of $149 - j22\,\Omega$. Because of mutual interactions occurring between the different dipoles and rings, the antenna impedance of these dipoles might be slightly different and therefore not perfectly matched at 600 MHz. Nevertheless, we expect the overall absorption to be larger than for just one single dipole-disk feed.

4.3.2 RCS analysis

The surface area of the dipole-disk array on which the incident field impinges is slightly larger than for that of the PEC plate and the horn feeds, due to the rings. The absorption and scattering on the other hand will be much different. The RCS over frequency of the dipole-disk array is presented in Figure 4.17, together with the RCS results of the PEC plate and the horn feed (with feedbox, without absorber).

These results show, and confirm, that the RCS of the dipole-disk array feed (at an angle of $\theta = 0°$) is smaller than the RCS of the plate and the horn feed. The horn feed absorbs part of the incident field due to the presence of the horn and therefore has a lower RCS than the PEC plate. The dipole-disk array feed has an even lower RCS over the 500-700 MHz frequency range, due to the multiple receiving elements.

To observe that indeed more of the incident energy is absorbed instead of scattered towards other θ directions, the RCS patterns of the three feeds over an angle of $\theta \pm 90°$ are presented in
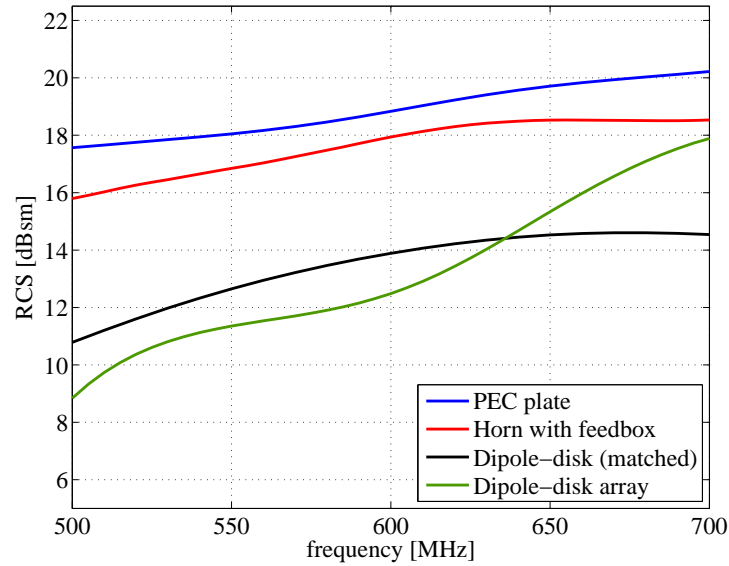
Figure 4.17: RCS over frequency for three different type of feeds with the same surface area towards the reflector ($\theta = 0°$).
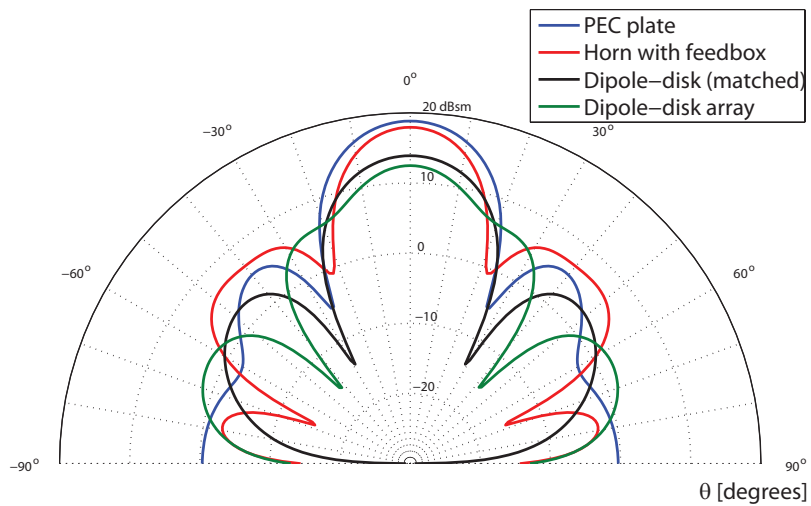

Figure 4.18: RCS patterns at 600 MHz over an angle $\theta = \pm 90°$ ($\phi = 90°$).

Figure 4.18. The RCS patterns are obtained at a frequency of 600 MHz and an angle $\phi = 90°$ (*E*-plane). The pattern of the dipole-disk array feed is indeed quite different from the others. Over an angle of $\theta = \pm 20°$, less of the incident field is reflected. In case of multiple reflections between the reflector and the feed, which are assumed to be mainly present within a small θ, the dipole-disk array feed has a lower RCS and therefore reflects less of the incident field.

4.4   Conclusion of feed analyses

In this chapter we have analyzed three different type of feeds, namely the dipole-disk feed, the horn feeds and the dipole-disk array feed. First the 1.695 GHz dipole-disk feed was analyzed. This is the same feed as was used for the parabolic reflector model in Chapter 3. By adjusting the radius of the disk, we have observed that change of RCS. From these results we have shown that smaller disks reflect less of the incident field, as we would expect. From the comparison of the RCS results of each feed with the estimated RCS values of the same sized PEC plate it could be observed that the RCS was lower, which is caused by the absorption of the feed. Together with the antenna gain results presented in Figure 3.10 which were obtained with the same dipole-disk, this has given us a good basis for further study.

The size of this dipole-disk feed was increased, in order for it to operate at a frequency of 600 MHz. The obtained RCS results of this feed can therefore be compare to those obtained from the horn feeds simulations. A feed operating at 600 MHz gives us also the opportunity of simulating an electrically large parabolic reflector, as it will be made clear in the next chapter. Several simulations were performed to analyze this feed with different port terminations to observe the absorption over the 400-800 MHz frequency range. At a matched load, the RCS again showed to be lower than the RCS of an equal sized PEC plate.

To obtain a good representation of the WSRT feed, a horn feed model was considered. This feed consists of a conical horn and is surrounded by a feedbox which has the same size as the WSRT telescope feedbox. We have chosen to simulate a simple horn feed instead of the corrugated horn feed which is used for the WSRT telescope. The simplified model has the same radiation pattern (approximately -13 dB normalized gain at 71°) as the corrugated horn and will also reflect part of the incident field due to the same sized feedbox which surrounds it.

We were able to reduce the RCS of the horn feed by placing the ECCOSORB® FGMU-125 wideband absorbing material to the surface around the horn aperture, without drastically changing its radiation pattern. The incident field would therefore impinge on a surface with the same size, but due to absorption less of the incident field will be reflected, resulting in a lower RCS. Different size absorber were used, to obtain feed with the same dimensions but different RCS.

The FPA is an example of a feed which has a low RCS [32]. To confirm that an increase of numbers of receiving elements lowers the RCS of a feed, we have chosen to analyze the dipole-disk array feed. The dipole-disk array is backed by a PEC plate which has the same surface area (towards the reflector) as the horn feeds. Our results have shown that the dipole-disk array reflects less of the impinging incident field by comparison to the RCS results of a PEC plate or horn feed (without absorber). The amount of elements (dipoles in our case) is not as large as for the FPA (Vivaldi elements). The RCS of the dipole-disk feed is therefore not as low as for the FPA, but we have shown that the RCS is lower than the RCS of a plate or horn feed. From this we conclude that the RCS of a feed can be decreased when more receiving elements are present. Beside the amount of elements, we have shown that the port termination of a feed (for example that of the 600 MHz dipole-disk feed) also influences that RCS. The right combination of antenna properties can therefore lead to a low amount of reflected energy.

The 600 MHz dipole-disk and the horn feeds will in the following chapter be simulated with the presence of an electrically large parabolic reflector. From those results, we will analyze their scattering behavior over frequency variations. Knowing that a feed with a lower RCS will reflect less of the impinging incident field, we hope to observe a change in antenna gain variation for different feeds.

Chapter 5

Reflector-feed simulations

In the previous chapters we have studied the standing wave phenomenon (Chapter 3) and analyzed several feeds with respect to their scattering and absorbing behavior (Chapter 4). From the results obtained with the (small) reflector antenna simulations in Chapter 3, Section 3.1, we have observed that the antenna gain fluctuates over frequency, such as is observed with the horn feed of the WSRT. In Chapter 4 horn feed models were analyzed. By placing an absorbing material on the surface of these feeds, the RCS in the direction $\theta = 0°$ of the feed was reduced. These feed models, together with the 600 MHz dipole-disk feed, were used for simulating the reflector-feed interaction in this chapter, to observe the antenna gain behavior over frequency. The research of Popping and Braun [11] showed that not only the antenna gain is affected by the standing wave phenomenon, but also the beamwidth of the WSRT. The -3 dB beamwidth will therefore in the following simulations also be observed.
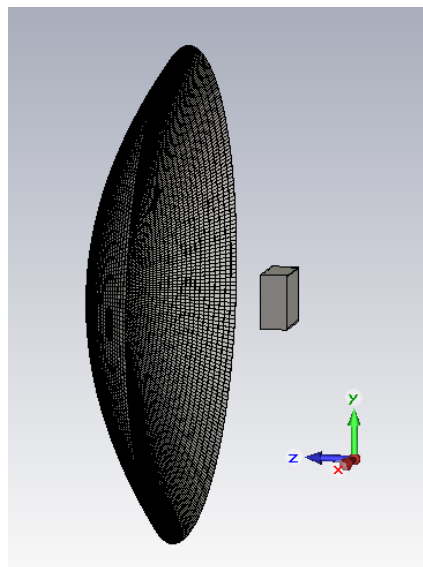

Figure 5.1: Parabolic reflector antenna model with horn feed.

For simulating an electrically large parabolic reflector reflector antenna, we have to investigate the possibilities of simulating a scaled WSRT model. A scaled WSRT model would probability experience the same reflector-feed interaction and therefore experience the same antenna gain fluctuation. Since the presence and absence of the antenna gain fluctuation has been observed with the WSRT telescope, a simulated model should also be able to show this feature. The WSRT parabolic dish has a diameter of 25 m and a focal length of 8.75 m. The frequency band used for the horn feeds is 500-700 MHz. Since the maximum required mesh stepsize (for the transient solver of CST) is $\lambda/10$, this stepsize would be approximately 4.3 cm at a frequency of 700 MHz ($\lambda \approx 43$ cm). A volume with dimensions N_x by N_y by N_z, where N is the number of steps, consists of 583 1/3 * 583 1/3 * 204 1/6 mesh cells (≈ 70 million). A model with this amount of mesh cells exceeds the available computational resources. After performing some simulations by down-scaling the reflector size and focal length of this model, we obtained a model having a parabolic reflector with a diameter of 10 m and a focal length of 3.5 m (where the WSRT F/D-ratio of 0.35 is kept) which we could solve on the most powerful computer to our disposal. The feed sizes are kept the same, since they are designed to operate at a specific frequency (range) and down-scaling them will change among others their radiation properties. Due to the need of extra accuracy, the mesh stepsize was later set to $\lambda/15$, ending up with a model size of approximately 15 million mesh cells ($N_x = 350$, $N_y = 350$, $N_z = 122\,1/2$. Around the reflector and feed extra space is added in the mode in CST, since the model boundaries in CST are set to 'open (add space)' in all directions. With the addition of this space the total amount of mesh cells of the simulated model is approximately 24 million. At a frequency of 600 MHz and a wavelength of 0.5 m, the reflector has a 20λ diameter and can therefore be considered an electrically large object.

The feed support legs, which are used to hold the feedbox in place, are initially not taken into account. Even though the presence of the support legs can have an influence on the multiple reflections between the reflector and the feed, the focus in this work lies on the reflections within the region between the apex of the reflector and the feed. With the FPA feed of the WSRT is has been observed that even with the presence of the support legs, the antenna gain fluctuation is not observable.
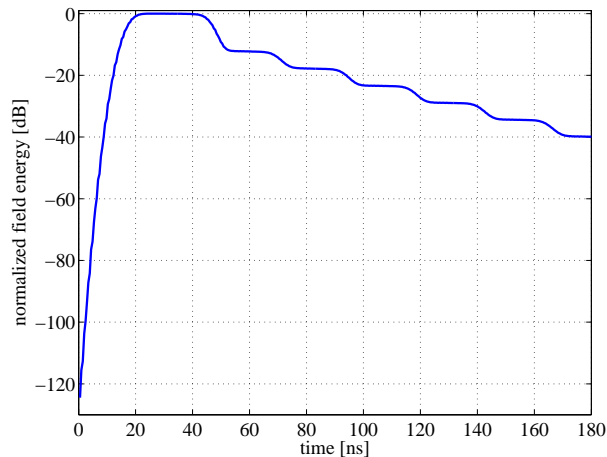

Figure 5.2: Energy decay over time for a simulation of the parabolic reflector antenna.

The model of the parabolic reflector antenna is presented in Figure 5.1. The dipole of the dipole-disk feed and the center of the horn aperture are placed at the focal point of the parabolic reflector. The phase center of these feeds vary over frequency, but are located along the z-axis and are locate around the focal point of the reflector.

The level of minimum normalized field energy for these simulations to end is set to -40 dB. As it can be observed from the results of the reflector and horn feed simulation (without absorber) in Figure 5.2, the simulation ends when the normalized field energy in the model reaches -40 dB. Each drop in field energy can be indicated with a reflection on the feed, where part of the field energy is reflected (back) by the feed and part is absorbed by the port or reaches the absorbing boundaries of the model.

5.1 Different feeds

The antenna gain results over frequency we present first are obtained with a dipole-disk feed, a horn (without feedbox) and horn feed without absorbing plate. From here on the horn feed will consist of a horn and a feedbox. Each feed differs in size (and shape), whereas it will reflection and/or absorb more or less of the incident field. What we would expect, and it is shown in Figure 5.3, is that for a feed with a smaller surface area on the side towards the reflector the gain variation is smaller. These results are obtained for the gain in the direction $\theta = 180°$, in which the maximum gain occurs.
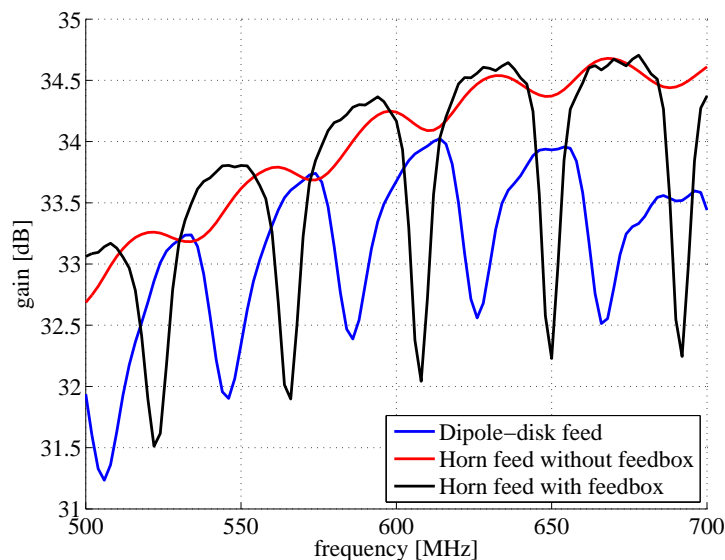

Figure 5.3: Antenna gain over frequency of the reflector antenna for different type of feeds ($\theta = 180°$).

From all the simulations results it can be observed that the gain fluctuates. Since the focal length of the reflector is 3.5 m, each successive minima occurs approximately every 43 MHz ($\Delta f = c/2F$). That for different geometries these minima do not occur exactly at the same

frequency is due to the fact that the incident field on the feeds are not reflected at the same point in space. The disk of the dipole-disk feed is positions at $z = -15$ cm and the front size of the feedbox at $z = 0$ cm. The reflected incident field of the horn and waveguide port also occur between $z = 0$ and 50cm.

5.2   Horn feeds

The RCS values of different horn feeds were analyzed in Chapter 4 and showed that with the presence of different size absorbers the RCS of the horn feed could be reduced. Four different configurations were used for the following reflector-feed simulation, namely a horn feed without an absorbing plate and with three different absorbing plate having different size (small, medium and large).
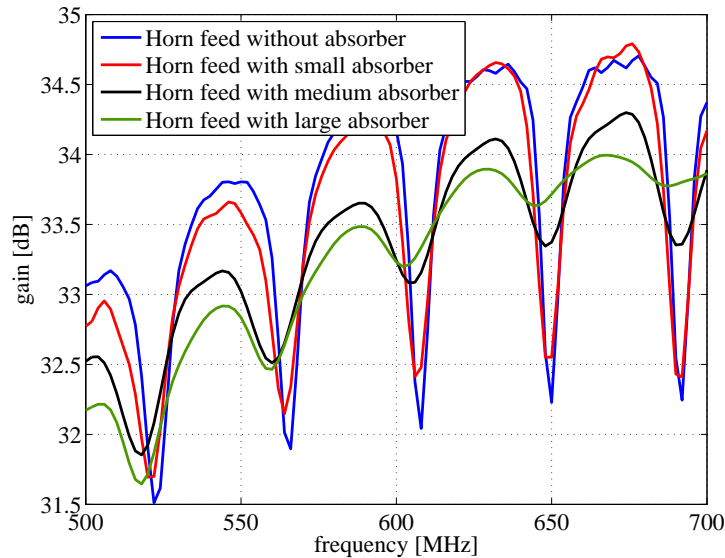
Figure 5.4: Antenna gain over frequency of the reflector antenna for different horn feeds ($\theta = 180°$).

Since the antenna gain is wavelength dependent [4], it increases with increasing frequency (within a certain limit). This can be observed in Figure 5.4, where the simulation results of the different horn feed configurations are presented. At those frequencies where standing waves occurs (a multiple of $\Delta f \approx 43$ MHz), the gain is significantly smaller for the feeds without an absorber and a small size absorbing plate. The antenna gain of these two feeds barely show any difference. Increasing the absorber plate from 35.1 % feedbox surface coverage (small size) to 63.5 % and 83.8 % coverage (medium and large size), results in a much smaller gain variation. The overall gain for these feeds is smaller, due to the fact that part of the incident field is absorbed by the absorbing plate, instead of being reflected. Since the incident field is mostly reflected at $z = 0$ cm, these antenna gain results show more overlap than the gain results in the previous section. A small difference can still be observed at the lower frequencies. This is due to

the fact that more field scatters inside the horn (feed with large absorbers), than at the surface of the feedbox (feed without absorber).

We are mostly interested in the harmonic gain variation and not so much in the gradual increase of antenna gain over frequency. The gradual increase of gain over frequency can be seen as the low-frequency component of a time-domain signal. By applying the same low-pass filtering technique which would normally be used on a time-domain signal, we have subtracted the gradual increase of gain over frequency. The gain variation we then obtain is presented in Figure 5.5(a). In Figure 5.5(b) the RCS over frequency of each horn feed is displayed. For frequencies at which standing waves occur between the reflector and the feed (multiple of $\Delta f \approx 43\,\mathrm{MHz}$), a drop in gain of about 1.5 dB is observed for feeds with an overall RCS higher the 10 dBsm (feed without absorber or with small absorber). The RCS of the feed with a medium size absorber is between 5 and 10 dBsm in the 500-700 MHz frequency range and shows to have much smaller gain variations (around 0.5 dB drop). The gain variation reduction of the large size absorber is again a little smaller ($\approx 0.25\,\mathrm{dB}$).
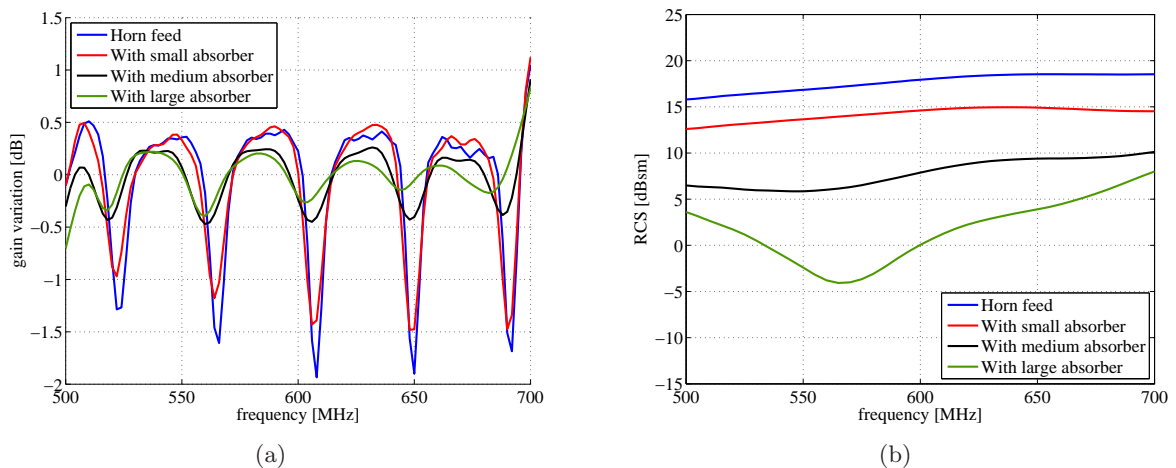

Figure 5.5: Comparison of results: (a) Antenna gain variation over frequency of the reflector antenna; (b) the RCS over frequency of each horn feed.

To get a better idea on how the RCS of the feed is related to the gain variation, we have taken a look at the peak-to-peak gain variations (difference between minimum and maximum gain) around several frequencies (515, 555, 600, 650 and 688 MHz). In Figure 5.6 the comparison of the gain variation at these frequencies versus the RCS is presented. The samples we have plotted here are obtained for the four different configurations (no/small/medium/large absorber). For each frequency four samples are used. From right to left the RCS versus gain variation of no absorber, small absorber, medium absorber and large absorber configurations are used. In case of the presence of a (larger) absorber the gain variation decreases for feeds with a lower RCS, as we have expected. The 600 MHz plot seams to be a good average compared to the other plots. In this case the gain variation drops about 0.17 dB per 1 dBsm in RCS.

If we look at how the -3 dB beamwidth of the reflector antenna changes over frequency for the different horn configurations, we should observe a overall decrease of beamwidth as the
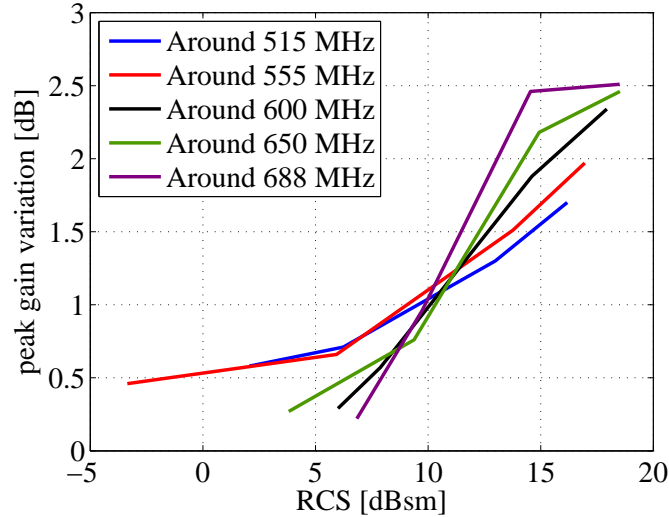
Figure 5.6: RCS versus gain variation.

frequency grows. This is due to the fact that the electrical size of the reflector becomes larger for smaller wavelengths and therefore more of the incident field is directed to towards the direction of maximum radiation ($\theta = 180°$). Since Popping and Braun [11] observed an variation of the beamwidth over frequency, we also expect to observe this effect in our simulations. In Figure 5.7 the -3 dB beamwidth (in the E-plane and absolute field value) over frequency of the different horn feeds (with and without absorbers) is presented. The increase of beamwidth of the parabolic reflector antenna caused by the standing waves is significantly reduced when feeds with a lower RCS are used. The mitigation of the multiple reflections between the reflector not only reduce the gain variation, but also the variation of the beamwidth. Where the calibration of the WSRT telescope is obscured by the variation of the main beam lobe over frequency, which they called *the heartbeat* of the WSRT telescope, a reduced feed RCS could overcome this problem.

To verify that the antenna gain variation and the beamwidth variation are both caused by the standing wave phenomenon, we have compared these two results in one graph for the medium and large size absorbers in Figure 5.8. Where the antenna gain is reduced due to the presence of the standing waves between the reflector and the feed, the beamwidth becomes larger. The local minima and maxima occur at those frequencies when standing waves occur. With the presence of a larger absorbing plate, the variations become smaller due to the mitigation of the reflection on the feed.

5.3 Feed support legs

In the beginning of this chapter we have mentioned that the WSRT telescope feedbox is held in place by support legs. We have assumed that the strongest reflections are mainly present directly between the apex of the reflector and the feed. The four support legs of the WSRT telescope are attached to the reflector at the angles $\theta = \pm29°$ and $\phi = \pm29°$ and therefore
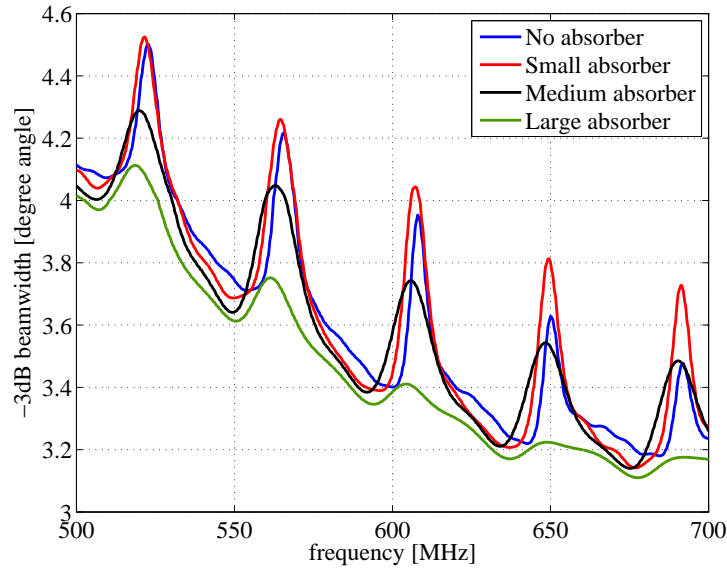
Figure 5.7: -3dB beamwidth of the reflector antenna for feeds without absorbing plate and with small, medium and large size absorbing plates.
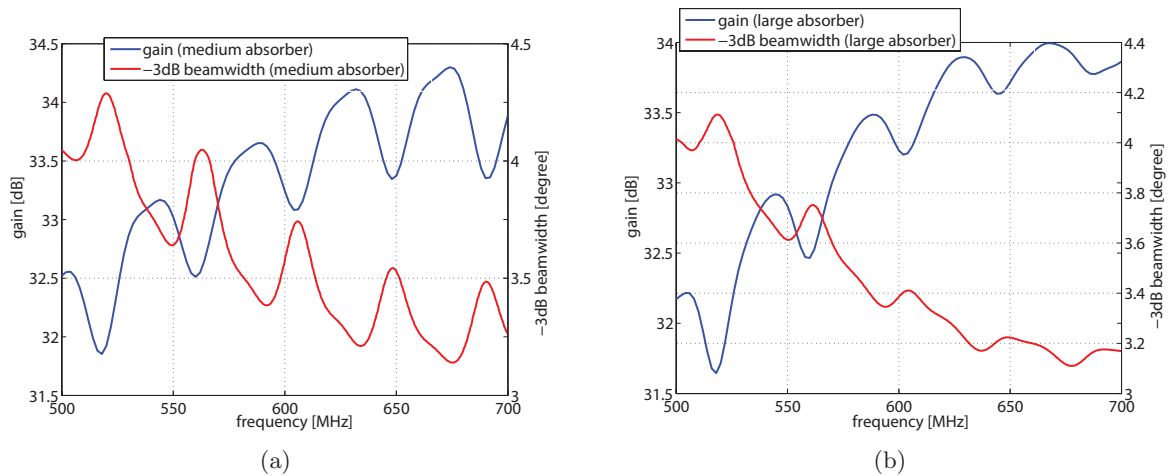

Figure 5.8: Antenna gain and -3dB beamwidth of the reflector antenna over frequency for a feed with: (a) a medium size absorbing plate; (b) a large absorbing plate.

not positioned near the direct path between the reflector apex and the feed. Since the support legs are attached to the feedbox near the focal point of the parabolic reflector, their length is approximately 3.5 m. To verify our assumptions about the small effect of the support legs on the antenna gain fluctuation, we have simulated a model with the presence of four support legs, as is presented in Figure 5.9.

The antenna gain variation over frequency is presented in Figure 5.10. Here we observe that the overall antenna gain of the model with support legs is lower, about 0.6 dB average, than
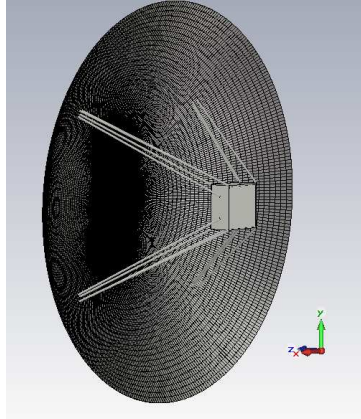
Figure 5.9: Reflector antenna model with feedbox and support legs.

the model without support legs. Their presence blocks part of the parabolic reflector aperture (shadow effect) and causes the gain to drop.
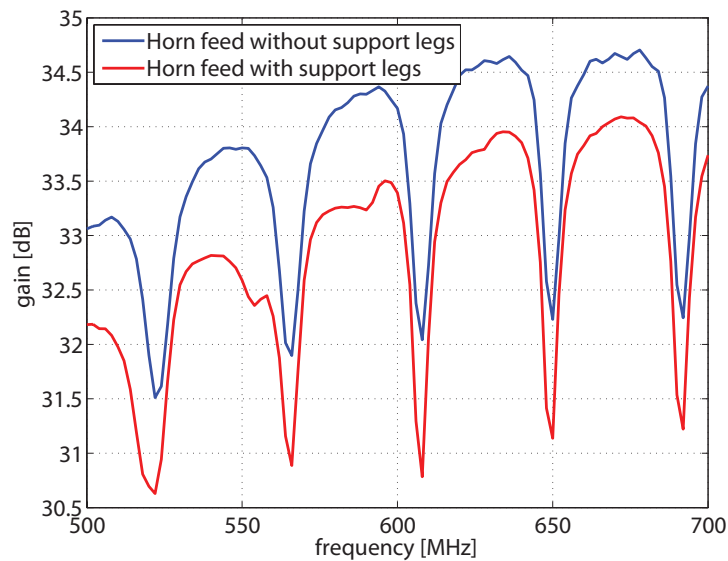

Figure 5.10: Antenna gain over frequency of the reflector antenna model with and without support legs ($\theta = 180°$).

In Figure 5.11 the gain variation over frequency for these two configurations is compared. Here we have subtracted the gradual increase of the antenna gain over frequency in the same way as in the previous section for the reflector-horn simulations. The magnitude of the variations shows a small difference, but is not as much affected as the magnitude of the antenna gain. We are mainly interested in the effect of the multiple reflections on the variation of the antenna gain over frequency. The support legs do not seem to contribute to this gain variation.

As for the reflector-horn simulation we have also taken a look at the -3 dB beamwidth of
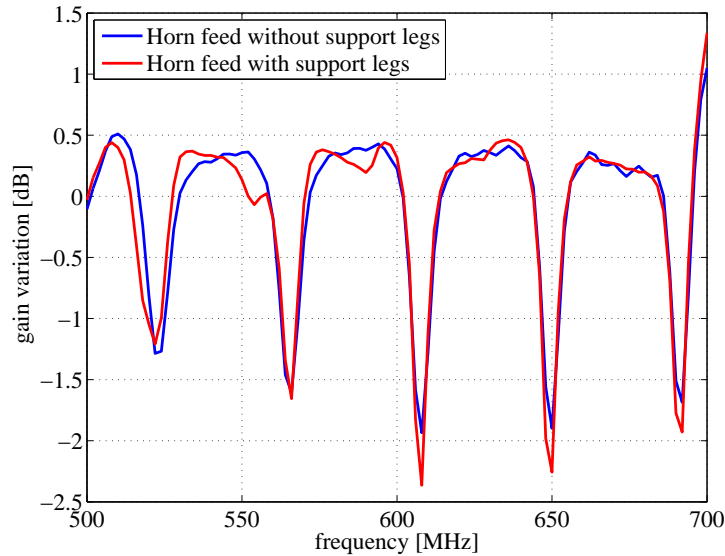
Figure 5.11: Antenna gain variation over frequency comparison of reflector antenna model with and without support legs.

the reflector antenna over frequency in the E-plane ($\phi = 90°$). In Figure 5.12 the beamwidth results obtained with a horn feed with and without support legs are presented. Even though the variation of the gain over frequency for both feed are quite similar, the beamwidth does vary. For the lower frequency (500-610 MHz), the -3 dB beamwidth is larger when support legs are presented, whereas for the higher frequencies (610-700 MHz) it is the other way around. Therefore we can conclude the presence of the support legs cause the variation of -3 dB beamwidth of the reflector antenna to decrease when the frequency grows, whereas the gain variation of the reflector antenna in the direction of $\theta = 180°$ is barely affected.

We have also compared the gain fluctuation and -3 dB beamwidth over frequency. As for the reflector-horn simulations, a clear agreement of changes in gain or beamwidth are observed, due to the presence of standing waves. In Figure 5.13 the comparison results of the simulations without and with support legs are presented.

5.4   Analysis of the results

In this chapter our goal was to simulate a large parabolic reflector antenna and to see how different feeds having different RCS levels would results in different gain fluctuations over frequency. Simulation of a real size model of the WSRT telescope was not feasible, due to its large dimensions. We did manage to simulate a parabolic reflector with a diameter of 10 m and a focal length of 3.5 m, which at an operating frequency of 600 MHz can be considered an electrically large object. The feeds we have used to illuminate this reflector have been studied in Chapter 4. Since the RCS of these feeds were examined, their behavior with respect to the multiple reflections between the reflector and the feed were analyzed in this chapter.
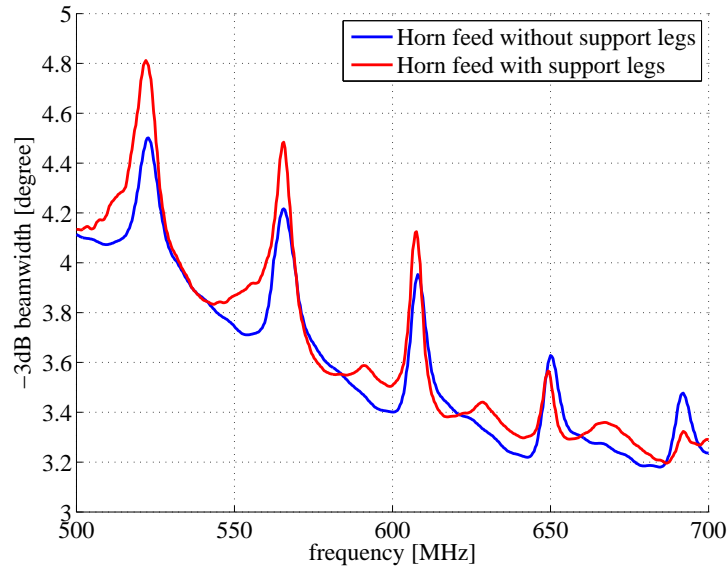
Figure 5.12: -3dB beamwidth of the reflector antenna with horn feed without and with support legs.
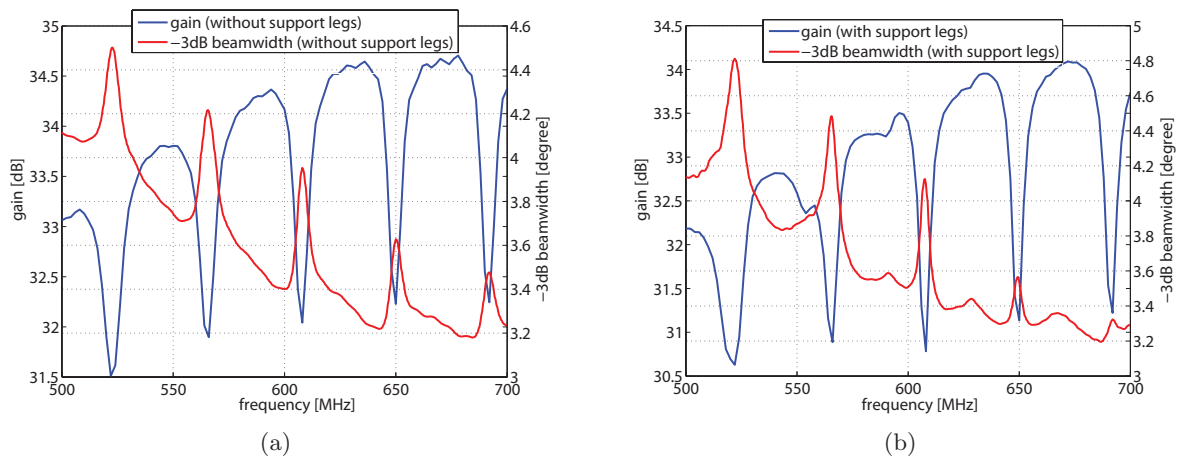

Figure 5.13: Antenna gain versus -3dB beamwidth of the reflector antenna over frequency: (a) absence of the support legs; (b) presence of the support legs.

The 600 MHz dipole-disk feed, together with the different horn feed configurations, were simulated with the presence of a parabolic reflector. The main results we have obtained from those simulations are the antenna gain variation of the reflector antenna over frequency and the -3dB beamwidth variation of the reflector antenna over frequency (in the E-plane). By using feeds with different RCS, mainly in the direction $\theta = 0°$, we wanted to observe a change (or elimination) of the antenna gain variation.

Our results have shown how the gain variation can be reduced, due to the mitigation of the reflections between the reflector and the feed, by using feeds with a lower RCS. We were also able

to almost eliminate the variation of the -3 dB beamwidth of the reflector antenna completely, which is in case of the WSRT telescope difficult to calibrate. For feed with an overall RCS larger then 10 dBsm, we have observed that the antenna gain drops significantly at frequencies where standing waves are present between the reflector and the feed. This drop in antenna gain is significantly reduced for feeds with a lower RCS, especially for the horn feed with a medium or large size absorbing plate, where the gain variation shows a sinusoidal behavior. The beamwidth is affected more than the antenna gain variations for the largest size absorbing plate. At higher frequencies the large variation of beamwidth is almost eliminated.

The FPA of the WSRT telescope has an RCS which is much smaller than the RCS of the horn feed with a large absorber. In this chapter we have shown that the gain variation is clearly reduced for feeds with a smaller RCS. From these finding we can conclude that the RCS of the FPA is small enough not to cause a significantly fluctuating antenna gain.

Chapter 6

Conclusions and recommendations

In this thesis we have analyzed the reflector-feed interactions occurring in prime-focus axial feed parabolic reflector antennas. By using the full-wave FDTD technique of CST we have simulated and analyzed the standing wave phenomenon, which is a plaguing phenomenon in (wideband) radio telescopes. With regard to the different feeds of the WSRT, we have analyzed several feeds to study their characteristic properties with respect to their scattering behavior. By examining the radar cross section of each feed we have investigated how this affects the antenna performance, namely the fluctuating antenna gain and the -3 dB beamwidth of the reflector antenna. Ways for mitigating the gain fluctuations over frequency, a consequence of the resonance effect present in the regions between the reflector and the feed, were suggested and assessed.

6.1 Conclusions

In Chapter 3 we have observed and visualized the presence of multiple reflections between the reflector and the feed in the case of the reflector antenna presented in [13]. Instead of the narrow operating frequency band it was designed for, we have simulated it over a wider frequency band. We have identified the presence of the standing waves and its relationship with the fluctuating antenna gain. For the first time a clear interrelation between the standing waves and the gain fluctuation, an interrelation previously suggested by several authors [6][10][11], was explicitly shown.

By investigating feeds with different port terminations we have observed the scattering behavior of the dipole-disk feed and how this affects the RCS. Not only is the absorption of the feed of importance, but also its scattering behavior. The RCS of different horn feeds were reduced by placing the ECCORSORB® FGMU-125 wideband absorbing material [30] around the horn aperture. Hereby we were able to reduce the scattering on the feed and therefore mitigate the multiple reflections in the region between the reflector and the feed. By using differently sized absorbing plates we have analyzed several horn feeds (with surrounding feedbox) and we have analyzed its scattering behavior. These dimensions of these feeds were fixed, but each had different RCS properties. The use of the absorbers is the first possibility to change the scattering

on a feed. Since some of the WSRT feeds are constantly being cooled to below 20 K, they are very sensitive to thermal noise and the presence of absorbers would therefore not be a viable option.

To verify that indeed an increasing amount of receiving elements can reduce the RCS of a feed, we have simulated and analyzed a dipole-disk array. As it was observed by van Cappellen [32] that the FPA has a low RCS (smaller than -20 dBsm). We have confirmed that an array configuration can reduce the RCS (pattern) of a feed and that it can therefore contribute to the mitigation of the multiple reflections.

Eventually we were able to simulate a parabolic reflector antenna with a diameter of 10 m and focal length of 3.5 m using the transient solver of CST. With a wavelength of 0.5 m (at 600 MHz) the diameter of the reflector has an electrical size of 20λ and a focal length of 7λ. It is therefore an electrically large objects. The electrical size of the WSRT telescope at 600 MHz was too large and a model of it could therefore not be solved with the computational resources we have to our disposal.

In Chapter 5 we have presented how the antenna gain of the parabolic reflector antenna fluctuates over frequency. We have demonstrated how the gain variation differs for different feeds. By changing the scattering properties of a feed, by means of reducing the RCS with the use of absorbers, we managed to mitigate the gain variations. The -3 dB beamwidth variation over frequency of the parabolic reflector antenna has also been investigated. From Popping and Braun [11] it was clear that the beamwidth of the main beam of the WSRT telescope varies over frequency (*the heartbeat*). Again we have demonstrated that that the -3 dB beamwidth variation can be reduced by using feeds with a lower RCS. Therefore we have proven that a feed with a lower RCS can minimize the multiple reflection in the region between the reflector and the feed and therefore reduce the gain variation and -3 dB beamwidth of the reflector antenna over frequency caused by the standing wave phenomenon.

We have finalized our research by observing the effect the feed support legs can have on the antenna performance. Initially we have assumed that the support legs do not contribute to the effect of the standing wave phenomenon, because they are not positioned in the region between the apex of the reflector and the feedbox. From our results we can conclude that the support legs affect the magnitude of the antenna gain, but not so much the variation of the antenna gain. The -3 dB beamwidth variation is affected more clearly due to the presence of the support legs. For an increase of frequency the standing wave phenomenon cause the beamwidth variation to decrease.

6.2   Recommendations

The scattering behavior of a feed for a parabolic reflector antenna is of great importance regarding the standing wave phenomenon. For the design of a feed for a wideband (parabolic) reflector antenna, the scattering behavior is an extra design criteria which should be taken into account. Ways to obtain this is by designing a feed or feedbox which would reflect most of an incident plane wave away from the apex of the reflector. Figure 6.1 is a simple example of how this can be achieved. We have discussed that the presence of absorbing material on the feed surface is

not preferable. Instead of an absorbing material, extra receivers could also absorb the incident energy. A mechanism to cool down these extra receivers would therefore be necessary, otherwise it would still cause thermal noise.
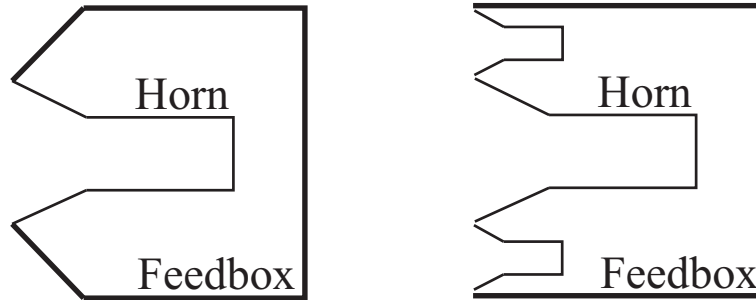

Figure 6.1: Strategic feed configuration.

Apparently, not all parabolic reflector antenna array feeds can eliminate the antenna gain fluctuation. The array feed which is under test at CSIRO in Australia [35] is an examples of this. It is therefore not apparent that an increase of antenna elements will eliminate the effect of the standing wave phenomenon. Also the design of an array feed is of importance, since increasing the number of receiving elements does not naturally lead the elimination or mitigation of feed scattering.

In our case we have used an axial feed parabolic reflector antenna. Other reflector antennas as an off-axis feed, a Cassegrain or a Gregorian reflector antennas also suffer from the standing wave phenomenon. Further study on these configuration might give a better understanding on how effective the RCS reduction of a feed is on the antenna performance.

Appendix A

Westerbork Synthesis Radio Telescope architecture

The Westerbork Synthesis Radio Telescope is an interferometric telescope which consists of a linear array of 14 radio telescopes arranged on a 2.7 km East-West line. One of the telescopes is shown in Figure A.1. Since it is equatorial mounted, parallel to the equator, it can follow the rotation of the sky by having one rotational axis parallel to the Earth's axis of rotation. Each telescope consists of a 25 meter parabolic reflector with a focal length F of 8.75 meter (F/D ratio of 0.35) and a primary focused feed held in place by four support legs. Each WSRT dish is equipped with a Multi Frequency Front End (MFFE), consisting of several corrugated horns, the low and high UHF systems. The operating wavelength and frequency are presented in Table A.1.

Figure A.1: Westerbork telescope

The MFFE is part of a feedbox with a front surface size of approximately 1.1 m by 1.1 m. This feedbox contained the receiving electronics, the cooling system and the feeds. A rotating

Type of receiver	Operating wavelength (cm)	Frequency range (MHz)	Polarization
Corrugated horn	92	310-390	dual, linear
Corrugated horn	49	560-610	dual, linear
Corrugated horn	18-21	1150-1750	dual, linear
Corrugated horn	13	2215-2375	dual, circular
Corrugated horn	6	4770-5020	dual, linear
Corrugated horn	3.6	8130-8650	dual, linear
UHW-low	-	250-460	dual, linear
UHW-high	-	700-1200	dual, linear

Table A.1: MFFE receivers of the WSRT telescope [18].

mechanism within the MFFE can place one of these horns (or two horns, if one is integrated into the other) in the receiving position.

Appendix B

Half wavelength dipole simulations

Besides the dipole-disk feed simulations we have also performed dipole simulations, in order to observe how the RCS of the feed changes over frequency. In Figure B.1 the half wavelength dipole model is shown. The operating frequency of the dipole will lie around $600\,\text{MHz}$ ($l \approx \lambda/2$). The radius of the dipole is $5\,\text{mm}$ (0.01λ).
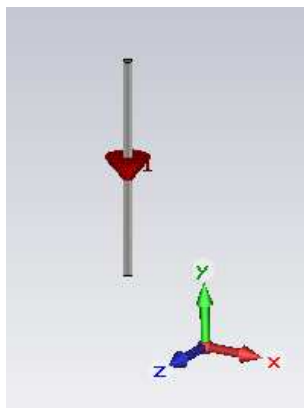

Figure B.1: Half wavelength dipole feed CST model

The antenna impedance Z_A of the dipole is presented in Figure B.2, where the antenna resistance R_A and the antenna reactance X_A are plotted over frequency. At a frequency of $600\,\text{MHz}$, the antenna impedance Z_A is $129.9 + j42.5\,\text{Ohm}$. For an ideal absorption of the dipole, the dipole port is terminated with an element with impedance of $129.9 - j42.5\,\text{Ohm}$ (matched load at $600\,\text{MHz}$, $R = 129.9\,\text{Ohm}$ and $C = 6.24\,\text{pF}$).

The RCS over frequency for different terminations is presented in Figure B.3. At at frequency of $600\,\text{MHz}$ the RCS is the highest. The absorption of the feed is at a maximum, but it re-radiates part of the incident field. In the case of an open circuit the RCS increases steadily over frequency and none of the incident field is absorbers or re-radiated. When the dipole is short circuited the highest RCS occurs at $500\,\text{MHz}$. At this frequency none of the incident field is absorbers, but re-radiation does take place. Figure B.4 shows how the RCS is equal in all θ directions.
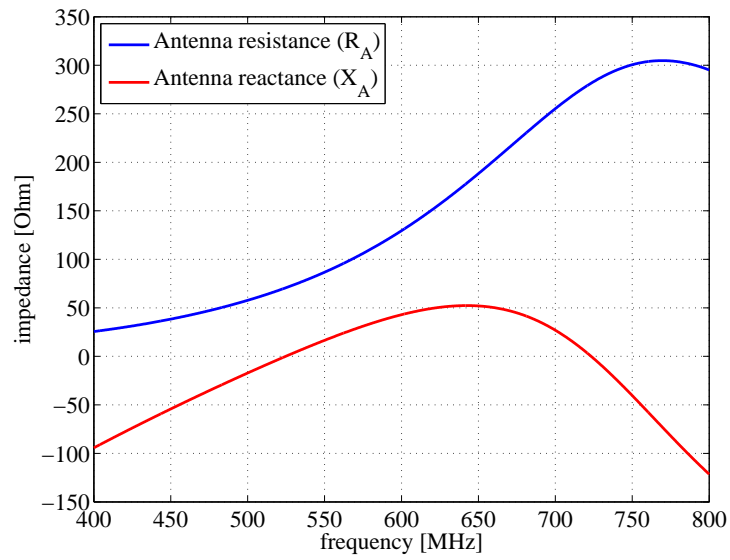
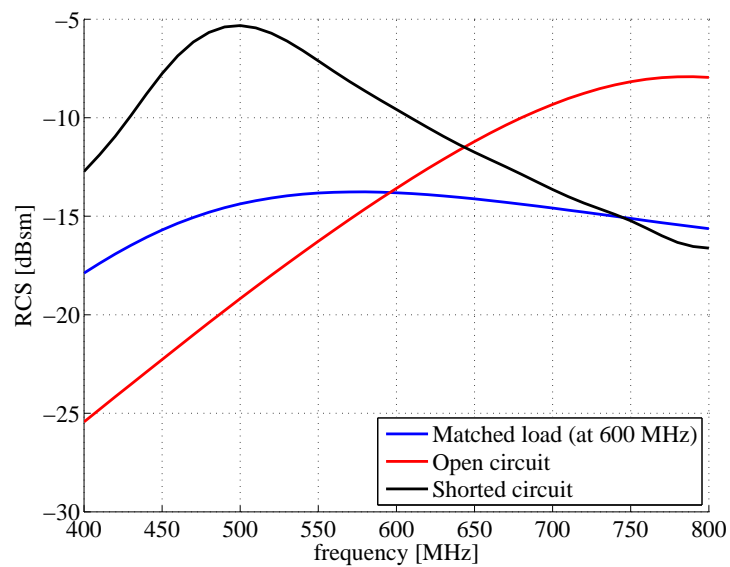Figure B.2: Antenna impedance of half wavelength dipole feed

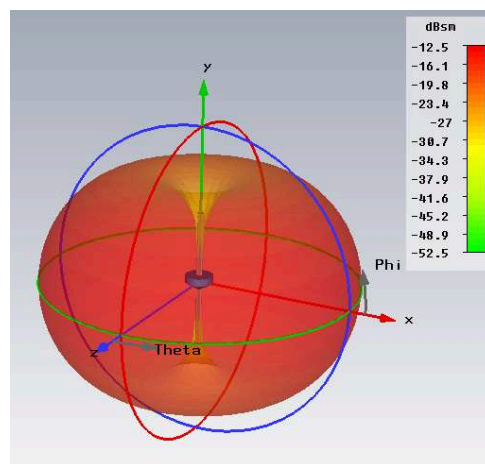Figure B.3: RCS over frequency for the dipole with different port terminations.

Figure B.4: RCS pattern of a matched load port termination at a frequency of 600 MHz .

Appendix C

Absorber simulations

The CST database contains several specific absorbing materials. The broadband absorbing material we have used is the ECCOSORB® FGMU-125 material [30]. The thickness of this material determines the amount of absorption, we have performed several simulations of different absorber thicknesses. We have defined a plate with size 1.1 m by 1.1 m, which is the same size as the front surface of the feedbox and the absorbing plate is backed by a PEC plate (see Figure C.1).
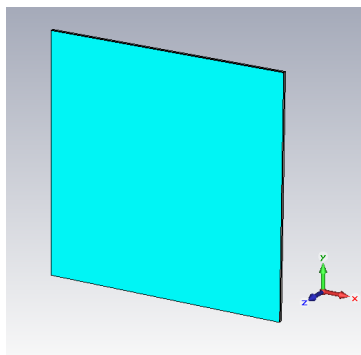

Figure C.1: Absorber CST model

The RCS results of each simulation are evaluated over a frequency range of 400-800 MHz and for absorber thicknesses of 8-10 mm. These results are compared to the estimated (with Equation 4.1) and simulated RCS results of a PEC plate. The absorbing plate with a thickness of 8.5 mm undergoes the highest absorption around 600 MHz and it therefore chosen for the horn feed simulations.
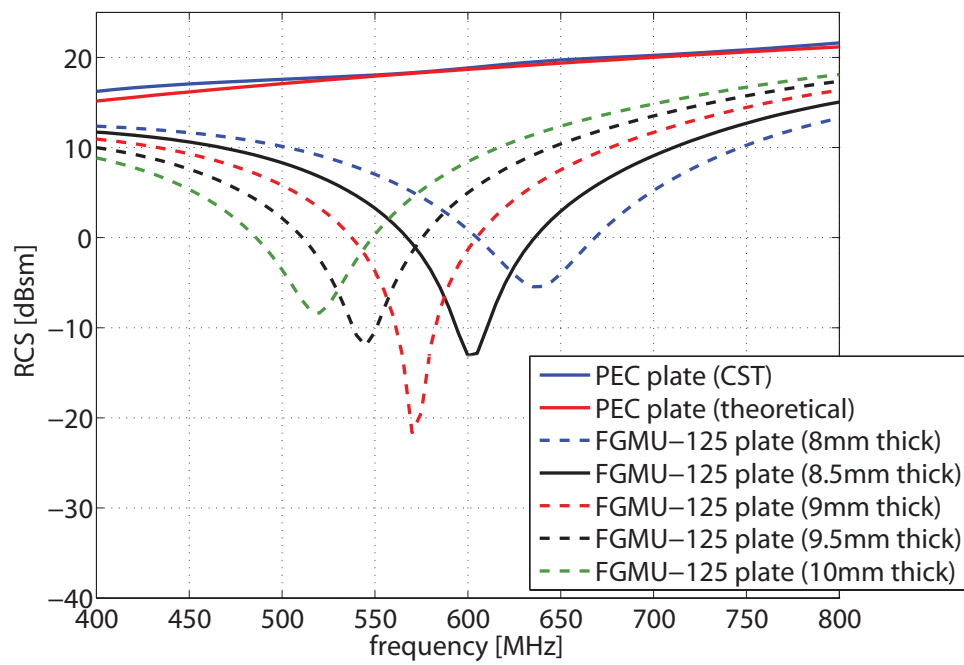
Figure C.2: RCS results of PEC and FGMU-125 absorbing plate with different thicknesses.

Bibliography

[1] http://www.setileague.org.

[2] H. I. Ewen and E. M. Purcell, "Observation of a line in the galactic radio spectrum," *Nature*, vol. 168, pp. 356–358, September 1951.

[3] C. J. Bakker and H. C. van de Hulst, "Radiogolven uit de wereldruimte ," *Nederl. Tij. Natuurkunde*, vol. 11, pp. 201–221, 1945.

[4] C. A. Balanis, *Antenna Theory*, Third Edition, Wiley-Interscience, 2005.

[5] A. A. Penzias and E. H. Scott III, "Intergalactic HI absorption at 21 centimeters," *The Astrophysical Journal*, vol. 153, pp. 799–801, July 1968.

[6] R. J. Allen, "The radio spectrum of Virgo A from 1411.7 to 1423.8 MHz," *Astron. Astrophys.*, vol. 3, pp. 316–322, August 1969.

[7] H. van. Woerden, "De neutrale waterstof in Orion," PhD Thesis, Rijksuniversiteit Groningen, July 1962.

[8] H. van Woerden, K. Takakubo and L. L. E. Braes, "Neutral hydrogen at intermediate galactic latitudes," *Bull. Astr. Inst. Netherlands*, vol. 16, no. 524, pp. 321–360, December 1962.

[9] E. Raimond, "21-cm Observations of two stellar associations in monoceros," *Bull. Astr. Inst. Netherlands Suppl. Ser.*, vol. 1, no. 2, pp. 33, 1966.

[10] F. H Briggs, E. Sorar, R. C. Kraan-Korteweg and W. van Driel, "Driftscan surveys in the 21cm line with the Arecibo and Nancay telescopes," *Publication of the Astronomical Society of Australia*, vol. 14, no. 1, pp. 37–44, January 1997.

[11] A. Popping and R. Braun, "The standing wave phenomenon in radio telescopes, frequency modulation of the WSRT primary beam," *Astron. Astrophys.*, vol. 479, no. 3, pp. 903–913, March 2008.

[12] http://www.astron.nl/dailyimage/index.html?main.php?date=20070205.

[13] P.-S. Kildal, "A small dipole-fed resonant reflector antenna with high efficiency, low cross polarization, and low sidelobes," *IEEE Trans. Antennas Propagat.*, vol. AP-33, no. 12, pp. 1386–1391, December 1985.

[14] A. Moldsvor and P.-S. Kildal, "Feed scattering in primary-fed reflector antennas," *Eur. Microwave Conf.*, Stockholm, Sweden, pp. 488-493, September 1988.

[15] A. Moldsvor and P.-S. Kildal, "Systematic approach to control feed scattering and multiple reflections in symmetrical primary-fed reflector antennas," *Proc. Inst. Elect. Eng.*, vol. 139, no. 1, pp. 65–71, February 1992.

[16] P.-S. Kildal, S. A. Skyttemyr and A. A. Kishk, "G/T maximization of a paraboloidal reflector fed by a dipole-disk antenna with ring by using the multiple-reflection approach and the moment method," *IEEE Trans. Antennas Propagat.*, vol. 45, no. 7, pp. 1130–1139, July 1997.

[17] P.-S. Kildal and Svein A. Skyttemyr, "Dipole-disk antenna with beam-forming ring," *IEEE Trans. Antennas Propagat.*, vol. 30, no. 4, pp. 529–534, July 1982.

[18] http://www.astron.nl/.

[19] M. V. Ivashina, J. Simons and J. G. Bij de Vaate, "Efficiency analysis of focal plane arrays in deep dishes," *Exp. Astrono.*, vol. 17, no. 1–3, pp. 149–162, 2004.

[20] M. A. W. Verheijen, T. A. Oosterloo, W. A. van Cappellen, L. Bakker, M. V. Ivashina and J. M. van der Hulst, "APERTIF, a focal plane array for the WSRT," *AIP Conference Proceedings*, vol. 1035 pp. 265–271, August 2008.

[21] W. A. van Cappellen, L. Bakker and T. A. Oosterloo, "Experimental results of a 112 element phased array feed for the Westerbork Synthesis Radio Telescope," *IEEE Symp. on Ant. and Propagat.*, Charleston, SC USA, pp. 1–4, June 2009.

[22] S. Silver, *Microwave Antenna Theory and Design*, McGraw-Hill, New York, Ch. 5, 1949.

[23] D. Morris, "Chromatism in radio telescopes due to blocking and feed scattering," *Astron. Astrophys.*, vol. 67, no. 2, pp. 221–228, July 1978.

[24] A. Heldring, "Full wave analysis of electrically large reflector antennas," Ph. D. dissertation, Delft Univ. Press, Delft, The Netherlands, April 2002.

[25] S. J. Franson, "Invited paper - Hybrid simulation of electrically large millimeter-wave antennas," *IEEE International Conference on Wireless Communications and Applied Computational Electromagnetics*, pp. 503–506, April 2005.

[26] P. Bolli, G. G. Gentili, L. Lucci, R. Nesti, G. Pelosi and G. Toso, "A hybrid perturbative technique to characterize the coupling between a corrugated horn and a reflector dish," *IEEE Trans. Antennas Propagat.*, vol. 54, no. 2, pp. 595–603, February 2006.

[27] http://www.feko.info/.

[28] http://www.ticra.com/what-we-do/software-descriptions/grasp/.

[29] http://www.cst.com/.

[30] (a) http://www.eccosorb.com/, (b) ECCOSORB® FGMU-125 wideband absorber: http://www.eccosorb.com/file/627/fgmu.pdf.

[31] M. I. Skolnik, *Introduction to Radar Systems*, Third Edition, McGraw-Hill, 2001.

[32] W. A. van Cappellen, "Beating down standing waves with APERTIF phased array feeds in the WSRT," *SKA2010 - International SKA Science and Engineering Meeting*, http://www.skatelescope.org/pages/SKA2010/ska2010.htm, March 2010.

[33] R. E. Collin, *Field Theory of Guided Waves*, Second Edition, Wiley-IEEE Press, New York, 1990.

[34] P.-S. Kildal, E. Olsen and J. A. Aas, "Losses, sidelobes, and cross polarization caused by feed-support struts in reflector antennas: design curves," *IEEE Trans. Antennas Propagat.*, vol. 36, no. 2, February 1988.

[35] CSIRO, www.csiro.au/group.